SUCCESSIVE JAHN-TELLER PHASE TRANSITIONS IN $K_2PbCu(NO_2)_6$

YUKIO NODA

August 1977

Contents

Synopsis

The successive phase transitions in $K_2PbCu(NO_2)_6$ has been studied by precise X-ray and neutron measurements. In phase II, we have observed the satellite reflections at ($H\pm0.416$, $K\pm0.430$, 0) around each fundamental Bragg reflection. In phase III, we have observed the superlattice reflections, instead of the satellite reflections of phase II, at ($H\pm\frac{1}{2}$, $K\pm\frac{1}{2}$, $L\pm\frac{1}{2}$). This fact indicates that the crystal undergoes the successive phase transitions as normal→incommensurate→commensurate phase.

The mode analysis of the Jahn-Teller active phonon mode was carried out and the experimental results were analysed from the standpoint of the condensation of the phonon mode. As the results, the phase transitions of $K_2PbCu(NO_2)_6$ crystal can be interpreted as sequencial cooperative Jahn-Teller transitions where the two degenerate $d\gamma$ electronic states of Cu^{2+} ion are split by the interaction with the transverse phonon mode at $\mathbb{k}_0=(0.42, 0.43, 0)$ in phase II and at $\mathbb{k}_0=(\frac{1}{2}\ \frac{1}{2}\ \frac{1}{2})$ in phase III.

§1. Introduction

The crystal of $K_2PbCu(NO_2)_6$ belongs to one of isomorphous system generally expressed as $R_2MCu(NO_2)_6$, where R=K, Rb, Cs, Tl, and M=Ca, Sr, Ba, Pb. These crystals contain octahedral $Cu(NO_2)_6$ complex in common. As is well known, Cu^{2+} ion in a cubic crystal field is Jahn-Teller active. Therefore, $Cu(NO_2)_6$ group has the tendency to become slightly distorted from the regular octahedron. Not only that, the crystal lattice itself would become distorted due to the cooperative effect of the interactions between the local distortions. The cooperative Jahn-Teller effect in $K_2PbCu(NO_2)_6$ is the central issue in this paper.

The properties of cooperative Jahn-Teller effect have been studied in various kinds of systems such as ferrites[1] ($FeNiCr_2O_4$, $CuNiCr_2O_4$), MnF_3[2], K_2CuF_4[3], Ba_2CuF_6[4] etc.. However, the system which we are concerned here, $R_2MCu(NO_2)_6$, has very interesting unique characteristics in the following points.

Firstly, some of them undergo 'successive'phase transitions due to cooperative Jahn-Teller effect. Generally speaking, successive phase transitions seem to occur more frequently in structural transitions than in magnetic transitions. One of this reason would be that the microscopic interactions which cause structural transitions have many varieties such as electrostatic interactions, Pauli repulsive forces, dispersion force etc.. Sequencial occurrence of several phase transitions is very interesting in that the order of sequence directly reflects the property of the microscopic interactions in the crystal. The $K_2PbCu(NO_2)_6$ crystal which we have studied in this paper is the typical case of showing

successive Jahn-Teller phase transitions.

Secondly, this system has an 'isolated' Jahn-Teller active groups; $Cu(NO_2)_6$ octahedra. In most of the Jahn-Teller systems which have been previously investigated, on the other hand, each Jahn-Teller active group is linked together by sharing anions with the neighbouring Jahn-Teller active groups. The existence of isolated Jahn-Teller group will make the system essentially simpler. At the same time, however, it may allow to introduce varieties in the possible pattern of lattice distortions because of the freedom of motions in the complex. For the later discussions, it should be pointed out that there are typically two possible types of local Jahn-Teller distortions in $Cu(NO_2)_6$ complex. The one is the case of the elongated tetragonal distortion of $Cu(NO_2)_6$ octahedron. This is the most commonly observed distortion in Cu^{2+} ion at octahedral site. The other is the case of the contracted tetragonal distortion, which has been reported to take place in some of the system of $R_2MCu(NO_2)_6$.

The last point is closely related to the above stated characteristics. As will be discussed later, the system of $R_2MCu(NO_2)_6$ seems to be categorized into two distinct classes. The one has pseudotetragonal unit cell with $c/a>1$. Namely, the unit cell is 'elongated' as compared with original (undistorted) cubic cell. The crystals of this class do not show any phase transitions in the observed temperature range. To this group, crystals with M=Ca, Sr, Ba belong. The other has also pseudotetragonal, but with $c/a<1$. Namely, the unit cell 'contracts' from regular cubic lattice. At the same time, the crystals of this type always show successive phase transitions. Crystals of $R_2PbCu(NO_2)_6$ with R=K, Rb, Cs belong

to this class.

By investigating the property of the successive phase transitions in $K_2PbCu(NO_2)_6$, we will submit some unified standpoint to interpret these overall features of Jahn-Teller effect in $R_2MCu(NO_2)_6$ system.

Before going into discussion of the property of $K_2PbCu(NO_2)_6$, let us summarize the structural data on this system in general. To begin with, we have given the structure of $K_2MNi(NO_2)_6$ with M= Ba[5] and Pb[6] in Fig. 1. Since Ni^{2+} is Jahn-Teller inactive, this crystal structure may be viewed as the 'prototype' structure to the distorted ones containing Jahn-Teller active group. This crystal has cubic symmetry (space group : Fm3) and $Ni(NO_2)_6$ group sitting at the corner of the cubic unit cell forms regular octahedron as expected.

The structural analysis of $R_2MCu(NO_2)_6$ series at room temperature are carried out extensively by Takagi et al.. In the case of Ca[10] or Ba[11], the structure is distorted from cubic prototype to orthorhombic (space group Fmmm). The lattice constants are, however, approximately tetragonal with $a \simeq b < c$*. That is, it has a pseudotetragonal unit cell with $c/a > 1$. The $Cu(NO_2)_6$ octahedron shows also elongated tetragonal distortion. The structural phase transition in this series has not been discovered.

---

* We choose the longest axis as an unique axis of the pseudotetragonal unit for convenience, although the lattice parameters are chosen as a>b>c in crystallographic convension.

The structure of $K_2PbCu(NO_2)_6$ at room temperature is analysed by Cullen and Lingafelter[12]. They concluded that the symmetry is cubic (space group Fm3) and $Cu(NO_2)_6$ group has regular octahedron. That is, it is isomorphous with Ni compound at room temperature. The structure of $R_2PbCu(NO_2)_6$, where R are Rb[13] or Cs[14], has lower symmetry at room temperature. Takagi et al. and Mullen et al. concluded that this series has also orthorhombic symmetry (space group Fmmm). However, in contrast to the case of M=Ca, Sr and Ba, the lattice has the compressed pseudotetragonal form and $Cu(NO_2)_6$ group is also considered to show contracted tetragonal distortion.

As is shown above, the structures of this system have been analyzed mainly at room temperature. Therefore, these only show the 'section' of variety of the structure at a fixed temperature. For instance $K_2PbCu(NO_2)_6$ is isomorphous with regular cubic structure. However, as temperature is varied, it exhibits more complex feature.

The crystal of $K_2PbCu(NO_2)_6$ undergoes two structural phase transitions successively at 280 K and 273 K. Starting from the highest temperature phase, let us call these three phases as phase I, II and III. We also name the transition temperatures as T_I (transition point for Phase I→Phase II) and T_N (transition point for Phase II→Phase III). The heat capacity[15] and the ESR experiments[16) 17] in the vicinity of these phase transitions have already been reported. From the ESR measurement, Harrowfield et al.[16] suggested that the $Cu(NO_2)_6$ group forms really contracted octahedron in phase II and in phase III and

that crystal lattice deforms to contracted pseudotetragonal lattice due to uniform arrangement of these contracted octahedra. Namely, they assumed 'ferrodistortive' ordering in low temperature phases. On the other hand, Reinen and his coworkers proposed an alternative model from their ESR experiments[17] as well as the anisotropy factor in thermal vibrations of NO_2 group in $Cs_2PbCu(NO_2)_6$[14]. Their model essentially assumes locally elongated $Cu(NO_2)_6$ octahedra. They proposed that in Phase II, the axis of elongation of each $Cu(NO_2)_6$ octahedra is oriented either one of the principal axes of the tetragonal basal plane at random. Namely, they characterized Phase II by two dimensional disorder with respect to the orientation of elongated octahedron (planar dynamic Jahn-Teller model). As for Phase III, they conjectured that in this phase, the $Cu(NO_2)_6$ complex is devided into two sublattices and the direction of elongation alternates between the a-axis and the b-axis in these sublattices. Namely, Phase III is considered to be the 'antiferrodistortive' ordered state. Recently, there has been hot debates between these two groups concerning whether it is ferrodistortive or antiferrodistortive order.[18),19)]

The purpose of the present work is to carry out the structure analysis precisely with X-ray diffraction and neutron diffraction measurements in lower temperature phases of $K_2PbCu(NO_2)_6$*, and to clarify the various aspects of Jahn-Teller phase transitions in $R_2MCu(NO_2)_6$ system.

---

* Preliminary data were already published in solid state comunication.[20),21)]

§II. Experimental

The single crystals of $K_2PbCu(NO_2)_6$ were grown from $6KNO_2$, $Pb(CH_3COO)_2$ and $Cu(NO_3)_2$. The 500 ml aqueous solution of $K_2PbCu(NO_2)_6$ added by a few drops of CH_3COOH was cooled with a rate of 0.2°C per day for 20 days, and then the single crystals of the size of 2~6 mm cube have been obtained. The crystal has dark greenish colour and the (111), (001) faces of the crystal develope most easily. The obtained crystals had the following properties. (i) The mosaicness of the crystals are less then 0.2° as measured by X-ray and neutron diffraction. (ii) The possible domain structure[5] at room temperature due to non-equivalence of cubic principal axes are not observed as discussed later. (iii) The transition temperatures T_I(phase I→phase II) and T_N (phase II→phase III) are consistent with other experimental results with errors less than experimental precision.

In this work, X-ray and neutron diffraction measurements with single crystal samples were carried out to investigate the precise feature of the successive phase transitions in $K_2PbCu(NO_2)_6$. In X-ray diffraction experiments, 40~50 KV×20 mA $CuK\alpha_1$ radiation which was monochromatized with pyrolytic graphite (PG) was used. In addition to usual method of Weissenberg photograph and scintillation counter, the position sensitive proportional counter (PSPC) was effectively utilized. The specification of PSPC which we have utilized is as follows: The flow gas is Ar-CH_4. The overall sensitive range of the counter is 10° in 2θ. The position of the incoming photons are analyzed by comparing the puls heights appearing

in both ends of the high resistive wire running along the axis of cylinder. The angle resolution is 0.04°. Further precise description of PSPC will be published elsewhere. In the neutron diffraction experiments, the triple axes TUNS diffractometer in JRR2 were used. The incident energy was 13.7 meV by monochromation with PG crystal. PG filter was also used to eliminate the contamination of the $\lambda/2$ component. The size of the used crystal was $4\times4\times7$ mm^3. The collimation of the spectorometer was 30'-30'-30'-30' between the reactor and monochromator, the monochromator and sample, the sample and analyzer, and the analyzer and detector, respectively. The energy resolution determined from the incoherent scattering of vanadium sample was 0.63 meV.

The crystal structure of phase I is well established by Cullen et al.[12] The space group of this crystal is determined as Fm3. Accordingly, due to the lack of the four-fold axes, the reflections with indices (hk0) and (kh0) are nonequivalent with each other. In fact the calculated intensity ratio of such the pairs as (420):(240) and (640):(460) considerably deviates from unity. The observed intensities of these reflections showed good agreements with the calculated intensity ratio both in the X-ray measurements and the neutron measurements. Whence we could choose the a-,b-, and the c-axes uniquely following Cullen's description.

The crystal undergoes two phase transitions successively. To see the overall feature of the phase change, we have performed precise X-ray measurements of the lattice constants using powder samples and single crystals. The observed temperature dependences

of the diffraction angle of $(12\ 0\ 0)_c$ and $(8\ 8\ 0)_c$ Bragg reflections are shown in Fig. 2. Here, $(hkl)_c$ means that the index refers to the cubic reciprocal lattice. Both $(12\ 0\ 0)_c$ and $(8\ 8\ 0)_c$ reflections show splittings in phase II, which shows that the unit cell transforms to tetragonal cell in this phase. The intensity ratio of the pairs after splitting measured by powder sample indicates $c/a<1$, namely, a contracted tetragonal lattice distortion.[10] In phase III, $(8\ 8\ 0)_c$ reflections show additional splittings implying the lattice belongs to the symmetry lower than orthorhombic. Further investigations of line splittings showed that the crystal system belongs to monoclinic cell in this phase. The unit cells of the crystal in each phase decided from these diffraction experiments are summarized in table 1.

Not only these changes in unit cells or in bulk distortions, we have observed additional characteristic reflections appearing in each phase . Namely, in phase I, we observed strong diffuse scatterings. In phase II, satellite reflections appear around each fundamental reflection . In phase III, these satellites disappear and instead of them new super lattice reflections are present. The features of the temperature dependences of these scatterings are summarized in Fig. 3. As shown in the figure, the first transition is strongly 1st order and the temperature hysteresis of transition is $\Delta T_I=1.6°C$. The second transition is also 1st order but the hysteresis is less than 0.1°C and looks more gradual than T_I. In the following, we describe the property of these three phases separately.

(A) Phase I; The fluctuation of Jahn-Teller mode.

In phase I, above the transition temperature T_I, the strong diffuse scattering intensity was observed by X-ray diffraction around each Bragg reflections, or the Γ-points in the Brillouin zone. The diffuse intensity shows moderate increasing when the temperature is decreased toward the transition temperature T_I and disappears suddenly upon transition to phase II. The intensity distribution of diffuse scattering were observed by PSPC around (8 8 0) in (h k 0) plane and (12 0 0) in (h l 1) plane. To obtain the diffuse scattering which are directly related to the critical fluctuations at the phase transition, the natural back ground and the thermal diffuse scatterings observed in phase II were subtracted from the observed diffuse intensity in phase I. The intensity contour around (8 8 0) and (12 0 0) are depicted in Fig. 4. The obtained diffuse scattering patterns in $K_2PbCu(NO_2)_6$ are essencially similar to the case of the Jahn-Teller phase transition in $NiCr_2O_4$[22], where the TA_1 acoustic phonon mode ($\mathbb{k}$//[110]) shows softening due to the cooperative Jahn-Teller effect. Therefore, we can infer that some soft phonon mode is expected to appear in the present case. The intensity of X-ray diffuse scattering due to acoustic phonons is given as

$$I_d \simeq I_f \left| \frac{\mathbb{K}\cdot e(s\mathbb{k})}{\omega(s\mathbb{k})} \right|^2 \qquad (1)$$

where $\mathbb{K}$ is the scattering vector, $e(s\mathbb{k})$ is the polarization vector of the phonon mode labeled with wave vector $\mathbb{k}$ and s, $\omega(s\mathbb{k})$ is the characteristic frequency of the phonon and I_f is the intensity of fundamental Bragg reflections. Comparing Eq. (1) with the

observed contours, especially noticing the strong anisotropy of the diffuse streaks which is running in [1$\bar{1}$0] direction around (8 8 0) Bragg reflection, we decided that the large fluctuations associated the phase transition is due to the transvers mode propagating along [110], and poralized along [1$\bar{1}$0], namely with $\mathbb{k}$//[110] and $\mathbb{e}$//[1$\bar{1}$0].

Preliminary measurements of the inelastic neutron scattering were carried out to check the existence of the soft phonon mode. We tried to observe phonons belonging to the TA_1 branch because the TA_1 mode is the lowest transversal mode and is considered to be the most important mode for the phase transition as discussed later. However, no well defined phonon peaks were observed in the range of $0.2 \leq \mathbb{k} \leq 0.6$. On the other hand, strong quasielastic scatterings centered at $\Delta E=0$ meV were observed as is shown in Fig. 5. The intensity distributions of the neutron quasielastic scattering ($\Delta E=0$ meV) were measured around (4 $\bar{4}$ 0), (4 $\bar{2}$ 0) and (4 0 0), the result being depicted in Fig. 6. The quasielastic scattering is running along [110] direction similar to the case of X-ray diffuse scattering. In Fig. 7 the drastic change of quasielastic scattering in energy and reciprocal space are demonstrated. Some data on the temperature dependences of the quasielastic scattering along the [110] line are shown in Fig. 8. The profiles show that there are shoulders around $\mathbb{k} \simeq$[0.3 0.3 0] in addition to the maximum point around $\mathbb{k} \simeq$[000], and the intensity of these scatterings increases as the temperature comes close to the transition temperature T_I.

(B) Phase II; Satellite reflections and the incommensurate structure.

Phase II of $K_2PbCu(NO_2)_6$ has a tetragonal lattice (c<a) as is described previously. However, this seems to an accidental case because any subgroup of phase I (space group Fm3) does not belong to tetragonal space group but has symmetry lower than orthorohmbic Fmmm. In this paper, we use the reciprocal lattice index of phase II referring to the tetragonal lattice which has the same unit cell size as phase I. When the temperature is cooled through the transition temperature T_I to phase II, the diffuse quasielastic scatterings around the Γ points suddenly disappear and, instead of them, the satellite reflections become observable in addition to the tetragonal bulk contraction. (See Fig. 2, Fig. 3 and Fig. 7.) The indices of the observed satellite reflections determined by neutron diffraction were $(H\pm0.416, K\pm0.430, 0)$. Based on this fact, phase II should be considered as an incommensurate phase where the lattice is modulated with the wave vector $\mathbb{k}_0=(0.416, 0.430, 0)$. The direction of $\mathbb{k}_0$ is very close to [110] direction of cubic unit cell and the position of $\mathbb{k}_0$ is close to the middle point between the two commensurate wave vectors, $(\frac{1}{2}\ \frac{1}{2}\ 0)$ and $(\frac{1}{3}\ \frac{1}{3}\ 0)$. The temperature dependences of the peak intensity as well as the position of the satellite reflection were precisely measured. However, no appreciable change in the position $\mathbb{k}_0$ and in the intensity of the satellite reflection were observed in this intermidiate phase. (See Fig. 2.) The intensity distribution of the satellite reflections measured by neutron scattering are shown schematicaly in Fig. 9-a. In this neutron experiment, the crystal of phase II happend to have almost complete ab domain in the equator with the ac and bc domains less than 10%. Therefore the indicated intensities should be indexed as

(hk0). The possibility of the existence of satellite reflections in (h01) plane and (0kl) plane were checked with X-ray measurements using PSPC around several Bragg reflections. As the result, the satellite reflections did not exist in (h01) and (0kl) plane within the accuracy given by $\langle I_s \rangle / \langle I_f \rangle \simeq 10^{-4}$ where I_s and I_f mean the intensity of the satellite and the fundamental Bragg reflections, whereas the observed satellite reflections on (hk0) plane show the intensity ratio $\langle I_s \rangle / \langle I_f \rangle \simeq 10^{-2}$. The existence of the second harmonics of the satellite reflections in (hk0) plane were also checked. The typical data of the satellite reflections observed with PSPC are shown in Fig. 10 and Fig. 11. In Fig. 10, (0, 12, 0) fundamental reflection, 1st satellite reflection at (0.42, 12.43, 0) and 2nd satellite reflection at (0.84, 12.86, 0) are shown. These profiles have been obtained by so-called ω-scanning integration method by fixing the 2θ angle of PSPC. The step scanning with the stepping angle of $\Delta\omega = 0.02°$ were carried out in the range of $\omega = \pm 0.2°$, and time shown in the intensity scale of the figure means the total time for the integration. The integrated intensity ratio for these reflections are $I_s(\mathbb{k}_0)/I_f \simeq 5.6 \times 10^{-2}$, $I_s(2\mathbb{k}_v)/I_s(\mathbb{k}_0) \simeq 5.3 \times 10^{-3}$, where the corrections for domain structure are considered as described later. In Fig. 11, satellite reflections around (0 12 0), ($\bar{4}$ 10 0) and ($\bar{8}$ 8 0) are given to demonstrate whether the frozen mode is TA like mode or LA like mode. The intensities of the satellites around ($\bar{8}$ 8 0) shows a remarkable contrast depending on the direction of $\mathbb{k}_v$ namely the intensities at ($\bar{8}$ 8 0)$\pm$(0.42, 0.43, 0) are strong while that of ($\bar{8}$ 8 0)$\pm$($\overline{0.42}$, 0.43, 0) are very weak which indicates

that the displacement of the atoms in the modulated structure is transversal.

(C) Phase III; superlattice reflections and the commensurate structure

As the sample is cooled further down to phase III, the satellite reflections at ($H\pm0.416$, $K\pm0.430$, 0) disappear and, instead of them, the superlattice reflections appear at $(H\pm\frac{1}{2}, K\pm\frac{1}{2}, L\pm\frac{1}{2})_c$ which is the L-zone boundaries of the 1st Brillouin zone. Namely the unit cell is doubled along each of the cubic principal axes. In this sense the lattice is considered to recover a commensurability in phase III. The temperature dependences of the integrated intensity of the $(-\frac{1}{2}\ 1\ 1\frac{1}{2}\ -\frac{1}{2})_c$ superlattice reflection were observed by X-ray diffraction. As shown in Fig.3, the intensity increases slightly as the temperature is decreased. The intensity distribution of the superlattice reflections as well as the fundamental reflections measured by X-ray are shown schematically in Fig. 9-b. The superlattice reflections shown in Fig. 9-b are the $(hkk)_c$ or $(hkh)_c$ type reflections. The $(hhl)_c$ type superlattice reflections are also observable but they are very weak especialy in X-ray diffraction pattern. The intensity distribution of some superlattice reflections were also measured by neutron diffraction with double axis method. The structure factor measured by X-ray and neutron diffraction will be analysed in the next section.

§III Analysis of the experimental results

A) mode analysis of the Jahn-Teller active phonon

It is well known that the 3d electronic state of Cu^{2+} ion in the octahedral crystalline field couples to the local distortions due to Jahn-Teller effect.[23] The electronic ground state is doublly degenerate $d\gamma$ orbitals having E_g symmetry. The local atomic vibrations with E_g symmetry which couple to the $d\gamma$ orbital are depicted in Fig. 12. In the figure, the local distortions which are conventionally called the Q_2- and the Q_3-mode are shown along with a rotational mode with T_g symmetry. These local distortions can be expanded with respect to the normal phonon modes in the crystal.

First, we investigate the L-zone boundary ($\mathbb{k}_0=\frac{1}{2}\ \frac{1}{2}\ \frac{1}{2}$) mode of Fm3 space group. The character table of the little group is shown in table 2. In the first column, the notations of irreducible representations by Kovalev[24], Koster and Mulliken[25] are listed. The normal coordinate was derived with the method given by Maradudin.[26] The irreducible representations of the L-zone boundary phonon mode in $K_2PbCu(NO_2)_6$ are

$$11L_1^+ + 11L_2^+ + 11L_3^+ + 11L_1^- + 11L_2^- + 11L_3^- \ . \qquad (2)$$

We are interested in the Jahn-Teller active phonon modes which are compatible with the local Q_2- or Q_3-mode. The Jahn-Teller active mode at L-zone boundary are identified as the L_2^+ and the L_3^+ mode. The normal coordinate of the L_2^+ and the L_3^+ are the complex conjugate with each other. Therefore we take the linear combination of L_2^+ and L_3^+ as the proper coordinate to represent real atomic displacements.

If we neglect the relative displacement of the oxygen against nitrogen of $Cu(NO_2)_6$, the numbers of the parameter for $L_2^+ \pm L_3^+$ normal coordinate decrease to 10 from 22. These parameters are listed in table 3. The most probable Jahn-Teller active mode is transverse mode which is polarized along $[1\bar{1}0]$ with $k_0=(\frac{1}{2}\ \frac{1}{2}\ \frac{1}{2})$, namely TA zone boundary phonon mode. Locally this mode is decomposed into the Q_2 type distortion (orthorhombic symmetry) and the rotational mode with T_g symmetry. The pattern of the mode at z=0 layer is depicted in Fig. 13-b.

Next, we try to carry out similar analysis on the Σ-line ($k=\zeta\zeta 0$) to clarify the structure of phase II. However, the Σ-line of Fm3 space group has only m_z as the symmetry element. In fact, the observed indices of the satellite reflections in phase II is $k_0=(0.416,\ 0.430,\ 0)$ which is very close to but not exactly on the [110] line. If we use Fm3 in order to perform the mode analysis, there are too many parameters left undetermined. Therefore we neglect oxygen for simplicity and use space group Fm3m. At the same time, we approximate the wave vector of the position of the satellite reflections as $k_0=(0.42,\ 0.42,\ 0)$. The character table of the little group of Σ-line of Fm3m is shown in table 2. As is shown in the table, we see that among lower frequency phonon branches, the LA-mode and the TA_1-mode are compatible with the local Jahn-Teller active modes. On the other hand, as previously stated, the observed intensity distribution of satellite reflections show that the frozen mode is of transverse character. Therefore, we infer that the most probable phonon mode which freezes in phase II is TA_1 mode. The pattern of atomic displacement of TA_1 mode at

$\mathbb{k}_0=(0.42, 0.42, 0)$ are shown in Fig. 13-a.

The Jahn-Teller active phonon mode which belongs to the irreducible representation of Σ_2 on [110] line or $L_2^+ \pm L_3^+$ at $(\frac{1}{2}\ \frac{1}{2}\ \frac{1}{2})$ point can couple to the local electronic state through electron-phonon interaction and as the result, these mode will become unstable at finite temperatures. The fluctuations due to these Jahn-Teller modes give the diffuse scattering in the scattering pattern in the highest temperature phase. As the temperature is lowered, these diffuse scatterings would become sharp satellite reflections or superlattice reflections in the lower temperature phases (phase II and phase III). If the structural modulation of lower phase is actually related to the freezing of an acoustic phonon mode, the intensity of satellite or superlattice reflections are roughly written as

$$I_s \simeq I_f \Sigma |\mathbb{k}\cdot\mathbb{\Delta}_j|^2 \ , \qquad (3)$$

where $\mathbb{\Delta}_j$ is the displacements of jth atom. In order to check the validity the observed intensity ratio I_s/I_f along [0K0] line measured with X-ray diffraction is plotted against $\mathbb{K}^2$ in Fig. 14. The ratio shows roughly linear relation against $\mathbb{K}^2$ in both phases. From this fact we can conclude that the lower phase is in fact related to the frozen structure of these Jahn-Teller active phonon mode.

B) structural analysis of phase II

The $K_2PbCu(NO_2)_6$ crystal has an incommensurate structure in phase II with the wave vector $\mathbb{k}_0=(0.416, 0.430, 0)$ or approximately $\mathbb{k}_0\simeq(0.42, 0\ 42, 0)$. For the incommensurate structure, the usual technique of a structural analysis is not applicable. Therefore

we tried to calculate the structure factor starting from the model of the phonon condensation discussed in the last section. The intensity ratio for the 1st and 2nd satellite reflections observed by X-ray measurements was 5.3×10^{-3}, which means that even if the 2nd satellites are due to the higher harmonics of the modulation, the ratio of amplitude of the 2nd harmonics versus the fundamental wave is about 7%. From this reason, we assume a purely sinusoidal modulation of the structure where the displacements of atoms are expressible as

$$\Delta_{\ell j} = \xi\, e_j(TA)\, \sin \mathbf{k}_0 \cdot \mathbf{r}_{\ell j} \ , \qquad (4)$$

where $\Delta_{\ell j}$ is the displacement vector of jth atom in ℓth cubic unit cell, ξ is the amplitude of the uniform transverse wave with polarization vector $e_j(TA)$ and $\mathbf{k}_0$ is the wave vector with (0.42, 0.42, 0). In addition to the transverse acoustic type displacements, we introduce sinusoidally modulated Jahn-Teller mode and rotational mode as follows :

$$\begin{aligned} \Delta_{\ell j} &= \Delta u_0 e_j(Q_3) + \Delta u_1 e_j(Q_3) \sin \mathbf{k}_0 \cdot \mathbf{r}_\ell \\ \Delta_{\ell j} &= \Delta v_1 e_j(Q_2) \cos \mathbf{k}_0 \cdot \mathbf{r}_\ell \\ \Delta_{\ell j} &= \phi e_j(T_{gz}) \cos \mathbf{k}_0 \cdot \mathbf{r}_\ell \ , \end{aligned} \qquad (5)$$

where Δu_1, Δv_1 and ϕ are the amplitude of the wave with the polarization vector $e_j(Q_3)$, $e_j(Q_2)$ and $e_j(T_{gz})$. Δu_0 is introduced from the evidence that the lattice of phase II has a uniformly contracted tetragonal distortion.

The structure factor of crystal is

$$F(\mathbb{K}) = \Sigma_j f_j e^{i\mathbb{K}\cdot r_{\ell j} + \Delta_{\ell j}}$$

$$\simeq \sum_n F_{fct}(\mathbb{K}_h)\ \delta\ (\mathbb{K} - (\mathbb{K}_h - n\mathbb{k}_0))\ F_n(\mathbb{K}) \qquad (6)$$

$$F_n(\mathbb{K}) = \sum_j f_j J_n(\mathbb{K}\cdot\xi e_j(TA))\ e^{i\mathbb{K}_h\cdot r_j}$$
$$+ \sum_j f_j J_n(\mathbb{K}\cdot\Delta u_1 e_j(Q_3))\ e^{i\mathbb{K}\cdot r_j}$$
$$+ \sum_j f_j J_n(\mathbb{K}\cdot\Delta v_1 e_j(Q_2))\ e^{i(\mathbb{K}\cdot r_j + \frac{\pi}{2}n)}$$
$$+ \sum_j f_j J_n(\mathbb{K}\cdot\phi e_j(T_{gz}))\ e^{i(\mathbb{K}\cdot r_j + \frac{\pi}{2}n)}\ , \qquad (7)$$

where f_j is the form factor of jth atom for X-ray or the scattering length for thermal neutron, $\mathbb{K}$ is the scattering vector and $\mathbb{K}_h$ is reciprocal lattice point, F_{fct} is the structure factor of face centered tetragonal lattice which is distorted from phase I due to Δu_0 (Q_3 uniform mode), and $J_n(x)$ is the n-th Bessel function. Eq. (6) gives not only the fundamental Bragg reflections and 1st satellite reflections but also the higher order satellite reflections. These higher harmonics are called as diffraction harmonics to distinguish from the higher harmonics in modulation.

To compare the observed intensity with Eq. (7) we made use of the temperature factors of phase I, and Δu_0 was determined from the bulk distortion. Thus the numbers of parameters to be determined are reduced to 8. The calculated structure factor for X-ray and neutron diffraction are shown in Fig. 15 along with the observed values. The R-factor is 6%, and the obtained parameters are listed in Table 4. The obtained parameter indicates that the most important component in the modulation is Q_2 mode as well as TA_1 like displacements. The displacement to $[\bar{1}10]$ direction are of order of 0.1Å which seems to be reasonable.

It is worthwhile to consider the two dimensional Q_2-Q_3 plane to characterize the distortion of $Cu(NO_2)_6$ octahedron. We have the modulated local distortion of the Q_2-mode as well as the uniform distortion of Q_3-mode. Therefore, the orientation of the arrows representing the local distortion is given by

$$\tan\psi = \frac{\sqrt{2}\Delta v_1(Q_2)}{\sqrt{6}\Delta u_0(Q_3)} = -2.48 \times \cos \mathbb{k}_0 \cdot \mathbb{r}_\ell \quad . \qquad (8)$$

Namely, in phase II the arrow changes its orientation from site to site. As is discussed in the later section, this feature may be characterized as having a 'fan' pseudospin structure. (See Fig. 19 (a).)

C) structural analysis of phase III

In phase III, we have observed the superlattice reflections at $(H\pm\frac{1}{2}, K\pm\frac{1}{2}, L\pm\frac{1}{2})_c$ in cubic indices. The extinction rule shows pseudomonoclinic space group C2/n(z=4). The real space group is $C\bar{1}$ (z=4) or $P\bar{1}$ (z=2) in primitive unit cell.

Since the structure of phase III is usual commensurate structure we could carry out the conventional structural analysis of crystals. However, if we start from the complete set of unknown parameters of space group $P\bar{1}$ (z=2), the numbers of parameters to be determined are 87 with isotropic temperature factors or 202 with anisotropic temperature factors. As an altanative, we start from the physically plausible model structure which can be deduced from the phonon mode analysis. The assumed displacements of the atoms are given by the same formulae as shown in Eqs. (4) and (5). Since $\mathbb{k}_0$ of phase III is $(\frac{1}{2}\ \frac{1}{2}\ \frac{1}{2})$, there are some different feature in the displacements given by Eqs. (4) and (5) between Phase II

and Phase III. Firstly, the TA type displacements of Cu^{2+} ion and Q_3 type modulation exactly vanish because of the symmetry of Phase III. Secondly, the distortion of $Cu(NO_2)_6$ octahedron and the displacements of Pb^{2+} and K^+ ion are considered as devided into two sublattices rather than having a modulated structure. The resulting model structure then belongs to the monoclinic space group C2/n if we neglect oxygens, which is consistent with the experimental results by X-ray diffraction. (See Fig. 16.)

The comparision of the calculated structure factors with the observed values are shown in Fig. 17, where R-factor is 12%. The obtained parameter are listed in Table 5. The displacement of each atoms is also listed in Angstrom unit. As is shown in the table the TA like displacements of nitrogen and oxygen atoms are decomposed to local Jahn-Teller Q_2-mode and rotational T_{gz}-mode. Namely, the obtained 6 parameters are interpreted as the local Q_2 type and the T_{gz} type distortions of $Cu(NO_2)_6$ octahedron as well as TA type displacements of Pb^{2+} and K^+ ions. As the most important result, we point out that the distortion of the $Cu(NO_2)_6$ octahedron at the origin of the unit cell shows the elongated tetragonal distortion with the axis of elongation along the $\vec{a}$-axis while $Cu(NO_2)_6$ at $(\frac{1}{2}\ \frac{1}{2}\ 0)$ is tetragonally elongated along the $\vec{b}$-axis. The configurational pattern of the elongated $Cu(NO_2)_6$ octahedron is essentially the same as Fig. 13-b, if we consider the arrows in the figure to be the displacements of atoms showing the tetragonal distortion. Therefore we concluded that the structure of phase III is characterized as 'antiferrodistortive' ordered state

of $Cu(NO_2)_6$ groups accompanied by the transverse displacements of Pb^{2+} and K^+ ions.

It is interesting to examine the character of this phase by describing the distortions in Q_2-Q_3 plane and compare with the characteristic feature in phase II. As is shown in Fig. 18, the position of Q_3^Z, Q_3^X and Q_3^Y on the circle means tetragonal distortion with the direction of elongation along Z, X and Y direction. The characteristic of the observed structure as explained above implies that the 'arrows' representing two sublattices point along Q_3^X and Q_3^Y directions. We calculated the direction of the local distortion for each sublattice on this circle from the observed value of Δu_0 and Δv_1. The result is shown as arrows in the figure. The angle ψ between the arrows representing two sublattices is $\pm 58.6°(3.2)$ from $-Q_3^Z$ axis.

D) domain structure in phase II and phase III

Crystal of $K_2PbCu(NO_2)_6$ has high symmetric cubic lattice in phase I. When undergoing the phase transitions, the symmetry of the crystal is lowered in phase II and phase III. Therefore, in the lower symmetry phases the crystal show domain structures as is usually the case. The phase transition of the crystal from phase I to phase II is accompanied by cubic to pseudotetragonal bulk distortion. As the result, the crystal can have three domains with its tetragonal axis along the cubic primal axis. This type of domains are easily distinguished by the diffraction angles of the Bragg reflections. The single domain crystal can be obtained when the crystal undergoes the transition under the existence of

external stress (stress cooled).

In phase II, four satellite reflections appear around the fundamental reflection with (H±0.416, K±0.430, 0). We label the position of these reflections as;

$$\begin{aligned} \mathbb{k}_1 &= (+\delta, +\delta, 0) \\ \mathbb{k}_2 &= (-\delta, +\delta, 0) \\ \mathbb{k}_3 &= (-\delta, -\delta, 0) \\ \mathbb{k}_4 &= (+\delta, -\delta, 0) \quad . \end{aligned} \tag{9}$$

$\mathbb{k}_1$ and $\mathbb{k}_3$ are related to each other by the inversion symmetry, while $\mathbb{k}_1$ and $\mathbb{k}_4$ are related to each other by the mirror symmetry on the b-plane of cubic lattice. The intensity ratio of the satellite reflections of the $\{\mathbb{k}_1, \mathbb{k}_3\}$ pair versus the $\{\mathbb{k}_2, \mathbb{k}_4\}$ pair showed variety depending on the experimental conditions. From this fact, the set of the satellites with $\{\mathbb{k}_1, \mathbb{k}_3\}$ and the set of $\{\mathbb{k}_2, \mathbb{k}_4\}$ are considered to belong different domains.

In phase III, the satellite reflections disappear and instead of them the superlattice reflections appear around the fundamental reflection with $(H\pm\frac{1}{2}, K\pm\frac{1}{2}, L\pm\frac{1}{2})$, namely, eight super lattice reflections appear around each Bragg reflection. These reflections are labeled as

$$\mathbb{k}_{n\pm} = \mathbb{k}_n \pm (0\ 0\ \tfrac{1}{2}) \quad , \quad n = 1, 2, 3, 4 \tag{10}$$

where $\mathbb{k}_n$ is the wave vectors of the satellite reflections discribed in Eq. (9) with $\delta=\frac{1}{2}$. In the similar way we have adopted to the satellite reflections, the superlattice reflections are divided into four type reflections as follows:

$$\{ k_{1+}, k_{3-} \} \quad , \quad \{ k_{1-}, k_{3+} \}$$
$$\{ k_{2+}, k_{4-} \} \quad , \quad \{ k_{2-}, k_{4+} \} \ . \qquad (11)$$

The set of $\{k_{1+}, k_{3-}\}$ can be indexed as the fundamental reciprocal lattice point of the unit cell:

$$\mathbf{a}' \simeq \frac{1}{2} [\bar{1}\ \bar{1}\ 2]_c$$
$$\mathbf{b}' \simeq \frac{1}{2} [1\ \bar{1}\ 0]_c$$
$$\mathbf{c}' \simeq \frac{1}{2} [1\ 1\ 2]_c \ . \qquad (12)$$

On the other hand, the set of superlattice reflections with $\{k_{2+}, k_{4-}\}$ belong to another unit cell:

$$\mathbf{a}'' \simeq \frac{1}{2} [1\ \bar{1}\ 2]c$$
$$\mathbf{b}'' \simeq \frac{1}{2} [1\ 1\ 0]_c$$
$$\mathbf{c}'' \simeq \frac{1}{2} [\bar{1}\ 1\ 2]_c \ . \qquad (13)$$

The pseudomonoclinic unique axes b' and b" are related by the mirror symmetry on the b-plane of the cubic lattice.

In Table 6, the possible indices of reflection arising from the domain structure are listed. The typical example of the domain structure which was observed around $(0\ 12\ 0)_c$ Bragg reflection is also given in the table. In this particular case, the set of $\{k_2, k_4\}$ was the dominant domain. The relation between the unit cell of each domain in phase III is also listed in the table.

§III Conclusions and discussions

The successive phase transitions in $K_2PbCu(NO_2)_6$ have been studied by precise X-ray and neutron diffraction measurements. The experimental results can be interpreted as sequencial cooperative Jahn-Teller phase transitions. In the intermediate phase, the local Jahn-Teller distortions are modulated with the wave vector $\mathbb{k}_0 \simeq (0.42, 0.43, 0)$. In the lowest temperature phase, it has an antiferrodistortive phase where the axis of local tetragonal elongation alternates from site to site. From the structural view point, the successive phase transitions in this crystal is characterized as normal→incommensurate→commensurate structural phase transitions, which is accompanied by cubic→ pseudotetragonal→pseudomonoclinic bulk deformation. On the other hand, the electronic state of the Jahn-Teller active Cu^{2+} ion is characterized as para→fan→canted pseudospin ordering.

We have analysed the structure of low temperature phases by X-ray and neutron measurements from the standpoint of phonon condensation. In this model we assume the condensation of TA as well as optical modes which is compatable with local Jahn-Teller distortion of $Cu(NO_2)_6$ groups with a transverse displacements. This model is considered to be fairly general because Δu_0 and Δv_1 are taken independently and whence any point on the circle in Q_2-Q_3 plane are allowed. We concluded that in phase III Pb^{2+} and K^+ ions show transverse displacements along $[\bar{1}10]$ direction and $Cu(NO_2)_6$ complex is distorted into tetragonally elongated octahedron whose

axis of elongation is oriented approximatelly to the a-or b-axis alternatively. We have obtained the value of $\psi=\tan^{-}\frac{\sqrt{2}\Delta v_1}{\sqrt{6}\Delta u_0} \simeq 59°$ on the Q_2-Q_3 circle while the purely 'antiferrodistortive' structure corresponds to the case of $\psi=60°$. On the other hand, if we neglect the term Δv_1 (Q_2-mode) in Eq. (5), the structural analysis will lead us to the values $\Delta u_0 \neq 0$, $\Delta v_1=0$ and $\phi>>0$, or the angle of $\psi=0$ on Q_2-Q_3 circle which means the 'ferrodistortive' with 'antiferrorotational' structure. From the results of least squre fitting of structural analysis, we conclude that the phase III is 'antiferrodistortive' structure.

We have also determined the structure of phase II. The structure is also characterized by the condensation of the same phonon mode, but with the wave vector which is incommensurate with the original lattice: $k_0 \simeq (0.42, 0.43, 0)$

In connection with this structure, the property of $R_2PbCu(NO_2)_6$ (R=Cs, Rb) is worthwhile to mention. The structural analysis of $Rb_2PbCu(NO_2)_6$ by Takagi et al.[13] and that of $Cs_2PbCu(NO_2)_6$ by Mullen et al.[14] at room temperature phase reported that both crystals have pseudotetragonal structure with space group Fmmm, and c/a<1 similar to the case of $K_2PbCu(NO_2)_6$. The obtained thermal factor of nitrogen atom showed a large anisotropy with large value along the Cu-N bonding direction. They considered therefore that this phase is disordered phase with the elongated tetragonal octahedron randomly oriented along the a-axis or the b-axis in ab plane. The contraction of the $Cu(NO_2)_6$ octahedron is considered as the result of 'time' average of dynamical Jahn-Teller effect. This model is

first proposed by Reinen et al.[17] from the ESR experiment. In the model, they characterized the successive phase transitions of $Cs_2PbCu(NO_2)_6$ crystal as follows; three dimensional disorder→ two dimensional disorder→antiferrodistortive ordering. On the other hand, if we neglect the satellite reflections observed in Phase II of $K_2PbCu(NO_2)_6$, the structure belongs to space group Fmmm with a pseudotetragonal lattice and the octahedron will have a contracted tetragonal form as the results of 'space' average of the sinusoidal modulation. We consider that this similarity is very interesting suggesting that the exact structure of these two materials might be the same as Phase II of $K_2PbCu(NO_2)_6$. The reexamination of the structure of $Rb_2PbCu(NO_2)_6$ and $Cs_2PbCu(NO_2)_6$ is necessary.*

---

* We have carried out a preliminary experiments for $Cs_2PbCu(NO_2)_6$ with X-ray diffraction. This system also shows successive phase transitions at T_I=391 (385)K and T_N=308K. The highest phase is determined as face centered cubic. In the lowest phase, we observed the superlattice reflections at L zone boundary similar to $K_2PbCu(NO_2)_6$. In the intermediate phase we observed the satellite reflections on the [$\zeta\zeta$0] line of the cubic unit cell. Therefore, the space group of low temperature phases are different from the space group Fmmm. However, the position of k_0 in phase II is exactly $\zeta=\frac{1}{2}$ which means that phase II has commensurate structure. We emphasize that the position of $[\frac{1}{2}\ \frac{1}{2}\ 0]$ in the Brillouin zone is not a special symmetry position. Therefore, the difference of k_0 between Cs compound and K compound is not a crucial one.

We try to infer the origin of the sequencial Jahn-Teller transition, with particular emphasis on the appearance of the incommensurate phase. We introduce the following Hamiltonian describing Jahn-Teller effects[2] with general wave vector $\mathbb{k}$;

$$\mathcal{H} = \sum_{\mathbb{k},s} g_{\mathbb{k},s} Q_{\mathbb{k},s} \sigma^x(\mathbb{k}) + \sum_{\mathbb{k},s} g_{\mathbb{k},s'} Q_{\mathbb{k},s'} \sigma^z(\mathbb{k}) \tag{14}$$

with

$$\sigma^x(\mathbb{k}) = \frac{1}{\sqrt{N}} \sum_{\ell} \sigma_\ell^x e^{i\mathbb{k}\cdot\mathbb{r}_\ell} , \tag{15}$$

$$\sigma^z(\mathbb{k}) = \frac{1}{\sqrt{N}} \sum_{\ell} \sigma_\ell^z e^{i\mathbb{k}\cdot\mathbb{r}_\ell} , \tag{16}$$

where σ_ℓ^x and σ_ℓ^z are the pseudospin operators associated with the local electronic state of the Jahn-Teller ion in the ℓ'th unit cell. Namely, they are represented by

$$\sigma^x = \begin{pmatrix} 0 & 1 \\ 1 & 0 \end{pmatrix} , \qquad \sigma^z = \begin{pmatrix} 1 & 0 \\ 0 & -1 \end{pmatrix} \tag{17}$$

when two $d\gamma$ orbitals of Cu^{2+} ion; $\psi_1 = x^2-y^2$ and $\psi_2 = 2Z^2-x^2-y^2$ are taken as the basis functions. $Q_{\mathbb{k},s}$ and $Q_{\mathbb{k},s'}$ are the amplitudes of the phonon normal modes with wave vector $\mathbb{k}$ and branch number s and s' which linearly couple to σ_ℓ^x's and σ_ℓ^z's. Similarly, $g_{\mathbb{k},s}$ and $g_{\mathbb{k},s'}$ are the Jahn-Teller coupling constants for the corresponding modes. Experimental results indicate that the important wave vector in the Hamiltonian are $\mathbb{k}=0$, $\mathbb{k}\cong(0.42,\ 0.42,\ 0)$ and $\mathbb{k}=(\frac{1}{2}\ \frac{1}{2}\ \frac{1}{2})$, namely Γ point, a point on Σ line, and L point in the Brillouin zone. From the results of the mode analysis and the structural analysis, we leave the following term in the Hamiltonian,

$$\mathcal{H}_1 = \sum_j g_0(\sigma^z\eta + \sigma^x\xi) \tag{18}$$

$$\mathcal{H}_2 = \frac{1}{\sqrt{N}}\left(g_{\Sigma_1}\sigma^z(\Sigma_1)Q_{\Sigma_1} + g_{\Sigma_2}\sigma^x(\Sigma)Q_{\Sigma_2}\right) \tag{19}$$

$$\mathcal{H}_3 = \frac{1}{\sqrt{N}}\left(g_{L,3}\sigma^z(L)Q_{L,3} + g_{L,2}\sigma^x(L)Q_{L,2}\right) \tag{20}$$

where ξ and η are the bulk distortions expressible in terms of elastic strain tensors as follows,

$$\xi = \frac{1}{\sqrt{2}}(e_{xx} - e_{yy}) \tag{21}$$

$$\eta = \frac{1}{\sqrt{6}}(2e_{zz} - e_{xx} - e_{yy}) \quad . \tag{22}$$

Q_{Σ_1} and Q_{Σ_2} are the phonon mode characterized by the irreducible representation at $k=(0.42, 0.42, 0)$, while $Q_{L,2}$ and $Q_{L,3}$ are the phonon mode at $k=(\frac{1}{2}\frac{1}{2}\frac{1}{2})$ which is compatible with the local Q_2-and Q_3-mode respectively.

Kanamori[2] investigated the cooperative Jahn-Teller transitions in ferrites ($CuFe_2O_4$, $CuCr_2O_4$, etc) and MnF_3 with Eq. (14) plus anharmonic term,

$$\mathcal{H}_{Anh} = -A_3(Q_3^2 - 3Q_3Q_2^2) + B_3[(Q_3^2 - Q_2^2)\sigma^z - 2Q_2Q_3\sigma^x], \tag{23}$$

$CuFe_2O_4$ and $CuCr_2O_4$ corresponds to the case of $k=0$ and MnF_3 to $k=(\frac{1}{2}\frac{1}{2}\frac{1}{2})$.

The situation of phase III in $K_2PbCu(NO_2)_6$ crystal is considered to be similar to the case of MnF_3 and is characterized as a canted pseudospin state. On the other hand, phase II in $K_2PbCu(NO_2)_6$ shows new aspect, namely the sinusoidal modulation of Jahn-Teller distortion leading to an incommensurate structure.

The appearence of the incommensurate phase as well as the existence of large fluctuation along [ζζ0] direction in the highest phase indicates that the coupling constant g_{Σ_2} is strong along a wide range of [ζζ0] direction, and the maximam position of the interaction energy is $k_0 \simeq (0.42, 0.43, 0)$ if commensurate energy is less than the Jahn-Teller energy. The sequencial appearence of Phase II and Phase III shows the relation of the magnitude of the coupling constants are $g_{\Sigma_2} \gtrsim g_L$.

To investigate Phase II in $K_2PbCu(NO_2)_6$, we rewrite the hamiltonian in the molecular field approximation using a fictitious pseudomagnetic field H,

$$\mathcal{H} = -\sum_{\ell} \sigma_{\ell}^{z} H_0^z - \sum_{\ell} \sigma_{\ell}^{x} H_{\Sigma,\ell}^{x} \tag{26}$$

where

$$H_0^z = -g_0 \langle \eta \rangle$$

$$H_{\Sigma,\ell}^{x} = -g_{\Sigma_2} \langle Q_{\Sigma,TA_1} \rangle \cos k_v \cdot r_{\ell} \quad . \tag{27}$$

As the fictitious field, we consider the tetragonal bulk deformation η and the displacement of TA_1 mode. The obtained Hamiltonian is formally equivalent to that which has been introduced by Yoshimori[27] for the herical spin system under the applied magnetic field, where H_0^z corresponds to uniform transverse field and H_{Σ}^{x} the staggered exchange field. From the analogy of the real spin system, we can expect that under suitable choice of parameters the 'fan' pseudospin state would be stabilized. From the stand point of

pseudospin ordering, the ordered state in Phase II and Phase III are considered as the fan pseudospin state and the canted pseudospin state respectively as is shown in Fig. 19.

Let us further discuss the general feature of Jahn-Teller effects in $R_2MCu(NO_2)_6$ system. As described previously, $R_2MCu(NO_2)_6$ crystal system can be divided into two groups. The material group of M=Ca, Sr and Ba belong to type A. They are characterized by the elongated $Cu(NO_2)_6$ octahedra with the elongated tetragonal lattice $c/a>1$ in the ordered phase. On the other hand, $R_2PbCu(NO_2)_6$ with R=K, Pb, Cs grouped as type B. They are characterized by the compressed tetragonal lattice ($c/a<1$) and also characterized by the existence of the successive phase transitions.

We try to classify these two groups. In Table 7 the bulk distortions as well as the local distortions in various materials are given, where Δu_a, Δu_b and Δu_c are the displacements of nitrogen atom from Cu-N distance u_0 of the regular octahedron, while Δa, Δb and Δc are the change in the lattice constants of original cubic axes. The values in parentheses are calculated ones by the condition that there is no volume change. We can extract the following characteristics from the table. (i) $c/a-1$ is about 4% for type A and -2% for type B. (ii) The magnitude of the lattice distortion

in type A is twice of type B. (iii) The displacements of nitrogen atoms of phase II have relationship among each other, namely, Δu_c of type B is equal to Δu_a of type A and Δu_a of type B is average of Δu_a and Δu_c of type A. These features are easily understood by attributing the following properties for each type, comparing with the displacements of phase III. Namely, $Cu(NO_2)_6$ complex in lower phase shows the tetragonally elongated octahedron with

$$\Delta u_c = -2\Delta u_a = -2\Delta u_b \simeq 0.17 \ \mathring{A} \qquad (28)$$

regardless of the type. However, type A has a ferro-type arrangement of the octahedron, while type B has antiferro-type arrangement. Therefore, the local distortion Δu is deduced from the normal mode Q_2 and Q_3 as follows:

$$(\text{type A}) \qquad \Delta u \Leftarrow Q_3^z \qquad (29)$$

$$(\text{type B}) \qquad \Delta u \Leftarrow \frac{1}{2}(Q_3^x + Q_3^y) \qquad (30)$$

Namely, we consider that in type A, octahedron is elongated along the c-axis by the $+Q_3^z$ mode in Fig. 18. On the other hand, in type B, it is elongated along the a-axis and the b-axis alternatively. We further consider that the lattice deformation is completely derived by the local distortion. Hence, the observed characteristics are deduced as

$$\begin{aligned} \Delta a &= 2\Delta u_a \\ \Delta b &= 2\Delta u_b \\ \Delta c &= 2\Delta u_c \end{aligned} \quad , \qquad (31)$$

where factor 2 is derived from the two displacements of NO_2 group of up and down and so on.

We can also consider the successive phase transitions of $R_2PbCu(NO_2)_6$ system from a unified view point. In Fig. 20, the 'phase diagram' is depicted, where the lattice parameter of cubic phase is taken as the vertical axis. The lattice parameters are taken from Table 7 and the transition temperatures are taken from the data in Friebel's paper.[28] The phase I, II and III is named in accordance with $K_2PbCu(NO_2)_6$ and the lines are drawn for the guide to eyes. The diagram shows overall relationship of the phases in this system. We may regard the vertical axis either as the concentration of the mixed crystal or as the uniaxial stress. In fact, the $K_2PbCu(NO_2)_6$ crystal is very sensitive for external stress and the single domain of phase II was easily taken as described in section III-E.

The diagram of Fig. 20 reminds us the P-T phase diagram of ammonium halides system.[29] The NH_4X system was characterized by the competition of two type interactions, where the direct interaction between NH_4^+ ion with octapole-octapole interaction and the indirect interaction between NH_4^+ ion via octopole-dipole interaction are important.

In the present paper, we concentrate ourselves to make clear the static structure which changes sequentially due to cooperative Jahn-Teller effect. On the other hand, the microscopic mechanism to cause the successive phase transition and to make the phonon modes with $\mathbb{k}_0=(0.42, 0.43, 0)$ and $\mathbb{k}_0=(\frac{1}{2}\frac{1}{2}\frac{1}{2})$ unstable are left for the future discussion. As the dynamical problem, we only observed the quasielastic scattering along $[\zeta\zeta 0]$ direction. The

precise measurements of phonon dispersion relation should be carried out to clarify whether the motion of Jahn-Teller active groups are diffusive motion or phonon-like propagative motion.

Acknowledgements

The author wishes to express his sincere thanks to Prof. Y. Yamada for his continual guidance and encouragement during the course of this study. Thanks are also due to Mr. Mori of Osaka University, Mr. Kashida of Niigata University and Dr. Fujii of Tokyo University for assisting experiments and the fruitful discussions. The author is pleased to acknowledge Miss T. Asakura for her effort in typing the manuscript.

References

1) M.Kataoka and J.Kanamori, J.Phys.Soc. Japan 32(1972)113

2) J.Kanamori, J.Appl.Phys. 31(1960)14S

3) R.Haegele and D.Babel, Z. anorg. allg. Chem. 409(1974)11

4) H.G.Shenering, Z. anorg. allg. Chem. 400(1973)201

5) S.Takagi and M.D.Joesten, Acta Cryst. B31(1975)1970

6) S.Takagi and M.D.Joesten, Acta Cryst. B31(1975)1968

7) J.A.Bertrand, D.A.Carpenter and A.R.Kalyanaraman, Inorg. Chem. Acta. 5 (1971)113

8) J.A.Bertrand and D.A.Carpenter, Inorg. Chem. 5(1966)514

9) S.Takagi and M.D.Joesten, Acta Cryst. B32(1976)326

10) S.Takagi, P.G.Lenhert and M.D.Joesten, J.Amer.Chem.Soc. 96(1974)6606

11) S.Takagi and M.D.Joesten, Acta Cryst. B31(1975)596

12) D.L.Cullen and E.C.Lingafelter, Inorg. Chem. 10(1971)1264

13) S.Takagi and M.D.Joesten, Acta Cryst. B32(1976)1278

14) D.Mullen, G.Heger and D.Reinen, Solid State Commun. 17(1975)1249

15) B.V.Harrowfield and R.Weber, Phys. Lett. A38(1972)27

16) B.V.Harrowfield and J.R.Pibrow, J.Phys.C 6(1973)755

17) D.Reinen, C.Friebel and K.P.Reetz, J.Solid State Chem. 4(1972)103

18) B.V.Harrowfield, Solid State Commun. 19(1976)983

19) D.Reinen, Solid State Commun. 21(1977)137

20) Y.Noda, M.Mori and Y.Yamada, Solid State Commun. 19(1976)1071

21) Y.Noda, M.Mori and Y.Yamada, Solid State Commun. 23(1977)247

22) H.Terauchi, M.Mori and Y.Yamada, J.Phys.Soc.Japan 32(1972)1049

23) M.D.Sturge, Solid State Physics (edited by F.Seitz, D.Turnbull and H.Ehrenreich) vol.20 p91. Academic Press, New York(1967)

24) O.V.Kovalev, Irreducible Representations of the Space Groups (translated from the Russian by A.M.Gross) Gordon & Breach, New York (1965)

25) C.J.Bradley and A.P.Cracknell, The Mathematical Theory of Symmetry in Solids, Clarendon press, Oxford (1972)

26) A.A.Maradudin and S.H.Vosko, Rev. Mod. Phys. 40(1968)1

27) T.Nagamiya, Solid State Physics (edited by F.Seitz, D.Turnbull and H.Ehrenreich) vol.20 p306. Academic Press, New York(1967)

28) C.Friebel, Z. anorg. allg. Chem. 417(1975)197

29) Y.Yamada, M.Mori and Y.Noda, J.Phys.Soc.Japan 32(1972)1565

Table captions

Table 1. Principal axes of the unit cell and the primitive cell of the three phases. The space groups were determined by X-ray measurements. The pseudosymmetries are also shown in the parentheses for the each phase.

Table 2. The character table of little group of Σ of Fm3m (O_h^5) and of L zone boundary point of Fm3 (T_h^3) space group.

Table 3. Normal coordinates of $L_2^+ \pm L_3^+$ mode. 10 parameters are still unknown based on this group theoretical analysis. As one of the choice of the parameters, TA like mode, Tgz like mode and Q_2 like mode are listed.

Table 4. The amplitudes of the 'phonon' in Phase II obtained by least square fitting method. Among these parameters, Δu_0 is determined from the measurement of lattice constants.

Table 5. (a) The amplitude of the 'phonon' in Phase III. The domain distribution was treated as an additional parameters in the least square fitting. (b) Displacements of each atom in Angstrom unit. $Cu(NO_2)_6$ octahedra at (0 0 0) site show elongated tetragonal distortion along the a-axis and that on $(\frac{1}{2}\ \frac{1}{2}\ 0)$ site along the b-axis.

Table 6. The indices to specify the satellite reflections and superlattice reflections belonging to different domains around $(0\ 12\ 0)_c$ Bragg reflection. For Phase III, pseudo-monoclinic indices are listed in the last column. The typical X-ray intensities of each reflection are also given.

Table 7. A table classifing $R_2MCu(NO_2)_6$ system with various structural parameters. The change of lattice constants and

the displacements of NO_2 group are summarized. References are given in section I. The values in the parentheses are the estimated values by the calcuration.

	unit cell	prim. cell	space group
Phase I	$a=[100]_c$ $b=[010]_c$ $c=[001]_c$ $z=4$	$a=\frac{1}{2}[110]_c$ $b=\frac{1}{2}[011]_c$ $c=\frac{1}{2}[101]_c$ $z_0=1$	Fm3 (Fm3m)
Phase II	$a'\cong[100]_c$ $b'\cong[010]_c$ $c'\cong[001]_c$ $a'=b'\neq c'$ $z=4$		incommensurate structure (Fmmm) (F4/m)
Phase III	$a'\cong\frac{1}{2}[\bar{1}\bar{1}2]_c$ $b'\cong\frac{1}{2}[1\bar{1}0]_c$ $c'\cong\frac{1}{2}[112]_c$ $\alpha'=\beta'=90°$ $\beta'\neq 90°$ $z=4$	$a'\cong\frac{1}{2}[110]_c$ $b'\cong\frac{1}{2}[011]_c$ $c'\cong\frac{1}{2}[1\bar{1}2]_c$ $\alpha',\beta',\gamma'\neq 90°$ $z_0=2$	$C\bar{1}$ ($C2/n$)

TABLE I

$O_h^5(\Sigma)$=mm2			E	$C_2 d$	m_z	md	local	phonon
τ_1	A_1	Σ_1	1	1	1	1	Q_3	LA
τ_2	A_2	Σ_3	1	1	-1	-1		
τ_3	B_1	Σ_2	1	-1	1	-1	Q_2 , T_{gz}	TA_1
τ_4	B_2	Σ_4	1	-1	-1	1	$T_{gx}+T_{gy}$	TA_2

$T_h^3(L)=\bar{3}$			E	C_3	C_3^2	I	S_3	S_3^2
τ_1	A_g	L_1^+	1	1	1	1	1	1
τ_3	^2E_g	L_2^+	1	ε	ε^2	1	ε	ε^2
τ_5	^1E_g	L_3^+	1	ε^2	ε	1	ε^2	ε
τ_2	A_u	L_1^-	1	1	1	-1	-1	-1
τ_4	^2E_u	L_2^-	1	ε	ε^2	-1	$-\varepsilon$	$-\varepsilon^2$
τ_6	^1E_u	L_3^-	1	ε^2	ε	-1	$-\varepsilon^2$	$-\varepsilon$

($\varepsilon=\exp(i\frac{2}{3}\pi)$)

TABLE 2

Atom	Δ_x	Δ_y	Δ_z
Cu	0	0	0
Pb	a_1	a_2	$-(a_1+a_2)$
K_1	b_1	b_2	$-(b_1+b_2)$
N_1	c_1	c_2	$-(e_1+d_2)$
N_3	d_1	d_2	$-(c_1+e_2)$
N_5	e_1	e_2	$-(d_1+c_2)$

(K_2, N_2, N_4, N_6); inversion for (K_1, N_1, N_3, N_5)

assume :

TA like

Cu	0	0	0
Pb	1	-1	0
K_1	1	-1	0
N_1	1	-1	0
N_3	1	-1	0
N_5	1	-1	0

T_{gz} like

N_1	0	1	0
N_3	-1	0	0
N_5	0	0	0

Q_2 like

N_1	1	0	0
N_3	0	-1	0
N_5	1	-1	0

site : N_1 = x 0 0

N_3 = 0 x 0

N_5 = 0 0 x

TABLE 3

	Amplitude (1/a)	Max. displace.
TA(K)	0.0091(8)	0.14 A
TA(Pb)	0.0023(5)	0.03
TA(Cu)	0.0210(21)	0.32
TA(N)	0.0068(8)	0.10
TA(O)	0.0109(8)	0.17
$\Delta u_o(Q_3)$	-0.0031	-0.03
$\Delta u_1(Q_3)$	0.0022(21)	0.03
$\Delta v_1(Q_2)$	0.0133(10)	0.13
ϕ (T_{gz})	0.0113(29)	0.6°

TABLE 4

a)

	Amplitude (1/a)	(Reduced)
TA(K)	0.0052(18)	
TA(Pb)	0.0035(3)	
TA(Cu)	0	
TA(N)	0.0081(17)	
TA(O)	0.0122(20)	
		Δu_o=-0.0031
$\Delta u_o(Q_3)$	-0.0031	Δv_1= 0.0088(14)
$\Delta u_1(Q_3)$	0	ϕ = 0.0253(71)
$\Delta v_1(Q_2)$	0.0041(11)	=(1.4±0.4°)
ϕ (T_{gz})	0.0015(46)	

b)

	site	displacements
Pb	$(\frac{1}{2}\ \frac{1}{2}\ \frac{1}{2})_c$	-0.038(3) [1$\bar{1}$0] A
	$\{\frac{1}{2}\ 0\ 0\}_c$	+0.038(3) [1$\bar{1}$0]
K_1	$(\frac{1}{4}\ \frac{1}{4}\ \frac{1}{4})_c$	+0.040(14) [1$\bar{1}$0]
K_2	$(\frac{3}{4}\ \frac{3}{4}\ \frac{3}{4})_c$	+0.040(14) [1$\bar{1}$0]
NO_2	(0 0 0)	Δu_o=2.111 A Δu_a=+0.119(19) A Δu_b=-0.061(10) Δu_c=-0.065
	$(\frac{1}{2}\ \frac{1}{2}\ 0)$	Δu_a=-0.061(10) Δu_b=+0.119(19) Δu_c=-0.065

TABLE 5

		Phase II	$\lvert F_{ob}\rvert^2$
	k_h	$(0 \quad 12 \quad 0)_t$	4548
A	k_1	$\delta \quad \delta \quad 0$	33
	k_3	$-\delta \quad -\delta \quad 0$	24
B	k_2	$-\delta \quad \delta \quad 0$	317
	k_4	$\delta \quad -\delta \quad 0$	219

$\delta = 0.42$

	Phase III		$\lvert Fob\rvert^2$	
	k_h	$(0 \quad 12 \quad 0)_c$	5640	$(\bar{+}6 \ \pm 6 \ 6)_m$
A'	k_{1+}	$\frac{1}{2} \quad \frac{1}{2} \quad \frac{1}{2}$	66	(-6 -6 7)
	k_{1-}	$\frac{1}{2} \quad \frac{1}{2} \quad -\frac{1}{2}$	37	(-7 -6 6)
	k_{3+}	$-\frac{1}{2} \quad -\frac{1}{2} \quad \frac{1}{2}$	15	(-5 -6 6)
	k_{3-}	$-\frac{1}{2} \quad -\frac{1}{2} \quad -\frac{1}{2}$	25	(-6 -6 5)
B'	k_{2+}	$-\frac{1}{2} \quad \frac{1}{2} \quad \frac{1}{2}$	560	(-6 6 7)
	k_{2-}	$-\frac{1}{2} \quad \frac{1}{2} \quad -\frac{1}{2}$	355	(-7 6 6)
	k_{4+}	$\frac{1}{2} \quad -\frac{1}{2} \quad \frac{1}{2}$	219	(-5 6 6)
	k_{4-}	$\frac{1}{2} \quad -\frac{1}{2} \quad -\frac{1}{2}$	306	(-6 6 5)

A' : $a' \simeq \frac{1}{2}[\bar{1} \ \bar{1} \ 2]_c$ B' : $a'' \simeq \frac{1}{2}[1 \ \bar{1} \ 2]_c$

$b' \simeq \frac{1}{2}[1 \ \bar{1} \ 0]_c$ $b'' \simeq \frac{1}{2}[1 \ 1 \ 0]_c$

$c' \simeq \frac{1}{2}[1 \ 1 \ 2]_c$ $c'' \simeq \frac{1}{2}[\bar{1} \ 1 \ 2]_c$

TABLE 6

(Lattice parameter)

		I	II		
		a_0	Δa	Δb	Δc
A	$K_2CaCu(NO_2)_6$	(10.461)	-0.136(2)	-0.143(2)	0.282(3)
	$K_2SrCu(NO_2)_6$		no ob.		
	$K_2BaCu(NO_2)_6$	(10.888)	-0.160(2)	-0.203(2)	0.331(1)
B	$K_2PbCu(NO_2)_6$	10.684(2)	0.066(2)	0.066(2)	-0.136(2)
	$Rb_2PbCu(NO_2)_6$	(10.754)	0.076(1)	0.066(1)	-0.143(1)
	$Cs_2PbCu(NO_2)_6$	(10.93)	0.11(1)	0.08(1)	-0.19(1)

(NO_2 displacements in $Cu(NO_2)_6$)

		I	II			III		
		u_0	Δu_a	Δu_b	Δu_c	Δu_a	Δu_b	Δu_c
A	$K_2CaCu(NO_2)_6$	(2.138)	-0.086(1)	-0.088(1)	0.175(1)		———	
	$K_2SrCu(NO_2)_6$			no ob.			———	
	$K_2BaCu(NO_2)_6$	(2.134)	-0.086(2)	-0.096(2)	0.177(2)		———	
B	$K_2PbCu(NO_2)_6$	2.111(4)	(0.03)	(0.03)	(-0.07)	0.12(2)	-0.06(1)	-0.07
	$Rb_2PbCu(NO_2)_6$	(2.136)	0.037(4)	0.037(4)	-0.073(3)		no ob.	
	$Cs_2PbCu(NO_2)_6$	(2.180)	0.047(8)	0.052(7)	-0.109(6)		no ob.	

TABLE 7

figure captions

Fig. 1 Schematic description of the structure of $K_2PbNi(NO_2)_6$ (space group : Fm3). To avoid complications, some of the atoms are omitted from the figure. The undistorted regular octahedra of $Ni(NO_2)_6$ group are sitting at the corner and at the face center of the cubic unit. This structure is considered as the prototype of the distorted phase of $R_2MCu(NO_2)_6$ system and $R_2MCo(NO_2)_6$ [7] system. The crystals of $K_2BaNi(NO_2)_6$, $K_2BaCo(NO_2)_6$ [8], $TlPbCu(NO_2)_6$ [9] and $K_2PbCu(NO_2)_6$ have been reported to be isomorphic with this structure.

Fig. 2 Temperature dependences of diffraction angles of $(12\ 0\ 0)_c$ and $(8\ 8\ 0)_c$ Bragg reflections referred to the cubic index. In phase II, each Bragg reflection splitts into two reflections to become pseudotetragonal lattice. The intensity ratio of these reflections indicates $c/a<1$. In addition to splittings at T_I(I→II), $(8\ 8\ 0)_c$ show further splittings at T_N(II→III) indicating lowering of the symmetry in phase III (pseudomonoclinic lattice).

Fig. 3 Temperature dependences of the intensity of diffuse quasielastic scattering with $k=(\zeta, \zeta, 0)$, the satellite reflections with $k_0=(0.42, 0.43, 0)$ and the superlattice reflections with $k_0=(\frac{1}{2}\ \frac{1}{2}\ \frac{1}{2})$. The sequencial phase transitions of $K_2PbCu(NO_2)_6$ are characterized by the properties of these reflections. In each case, the open circles indicate the data on heating and the solid ones on cooling.

Fig. 4 The intensity contour of the diffuse scattering

observed by X-ray measurements in phase I. The diffuse intensities around (12 0 0) in (h 1 1) plane and around (8 8 0) in (h k 0) plane are given. To observe these intensity contour, PSPC was utilized. The thin lines in the upper picture mean the range of the simultaneous observation by PSPC (10° in 2θ). Background was measured in phase II (275 K), and subtracted from the intensity contour measured in phase I (288 K). Hatched part of the picture near the Γ-point indicates the part where the subtraction is not possible because of the contamination by the other Bragg reflection appearing by the existance of the domain structure. The resolution function in this measurements was 0.01×0.01 in the horizontal plane and 0.01 in the vertical direction in the unit of the reciprocal lattice.

Fig. 5 Typical data of the measurements of TA_1 phonon mode in phase I along [110] direction. No well defined phonon peaks are observed. Instead of them, the large components centered at ΔE=0 meV have been observed.

Fig. 6 The intensity contour of the neutron quasielastic scattering in phase I (ΔE=0 meV). Intensity distributions around (4 0 0), (4 $\bar{2}$ 0) and (4 $\bar{4}$ 0) Bragg reflections in (h k 0) plane are shown. The doted points are the points where the measurements have been carried out. The ellipse at the Γ-point means the experimental resolution function.

Fig. 7 Temperature dependences of the spectrum of quasielastic

scattering at the reciprocal point (3.8, -2.2, 0), and the distribution in the reciprocal space along (4+ζ, -2.2, 0) at the ΔE=0 meV.

In phase II, the diffuse quasielastic scatterings disappear completely in both the energy and the momentum space.

Fig. 8 Temperature dependences of the quasielastic scattering along [ζ, ζ, 0] line.

Fig. 9 (a) The intensity distribution of satellite reflections measured by neutron diffraction and (b) the superlattice reflections measured by X-ray diffraction. The solid circles indicate the satellite or the superlattice reflections and the open circles indicate the fundamental reflections. For phase III, the reflections belonging to one domain are depicted.

Fig. 10 The 1st satellite reflection at (0.42, 12.43, 0) and the 2nd harmonics at (0.84, 12.86, 0) measured by PSPC. The channel number in the figure corresponds to the diffraction angle 2θ (0.04°/1 channel). The position of the counter were adjusted so that the 125th channel becomes the position of the given Bragg reflection.

Fig. 11 The intensity ratio between the satellite reflection and the fundamental reflection for several reflections. The method of the measurements are the same as Fig. 10. Equidomain for (0.42, 0.43, 0) and (-0.42, 0.43, 0) are assumed. The intensity of $(\bar{8}\ 8\ 0)+(\pm 0.42, 0.43, 0)$ (indicated by open circles and solid circles) correspond to the transversal components and the longitudinal components of the modurated structure propagating along [110] direction

respectively.

Fig. 12 The local mode of the octahedral molecule in m3m point group. Two degenerated vibrational mode (E_g symmetry) which are convensionaly called as Q_3-mode and Q_2-mode are shown along with the z-component of three degenerated rotational mode (T_g symmetry).

Fig. 13 The relevant atomic displacement pattern of phonon mode in z=0 layer of cubic unit cell. The displacements of K^+ ions are not shown. The upper figure shows the TA_1 phonon mode with $\mathbb{k}_0=(0.42, 0.42, 0)$ belonging to the irreducible representation of Σ_2. The lower figure shows the TA zone boundary phonon mode with $\mathbb{k}=(\frac{1}{2}\ \frac{1}{2}\ \frac{1}{2})$. The $Cu(NO_2)_6$ octahedra in both figure show the distortion similar to the local Jahn-Teller distortion.

Fig. 14 (a) The intensity ratio between satellite and fundamental reflections and (b) between superlattice and fundamental reflections observed by X-ray diffraction along [0k0] line. The correction for domain distribution are not mode. The linear dependence of the ratio indicates that the condneced mode in phase II and phase III are concerned with TA mode.

Fig. 15 Comparison of the calculated structure factors of the satellite reflections ($\mathbb{K}_h \pm \mathbb{k}_0$) with the observed values by X-ray and neutron diffraction in Phase II. Fundamental and 2nd satellite reflections are also included. R-factor is 6% (12% for satellite reflections) with 8 parameters. The

unit of neutron structure factor is 10^{-13} cm.

Fig. 16 The model structure of phase III. The displacements of K^+ ion and Pb^{2+} ions are shown by the arrows. The local distortion of $Cu(NO_2)_6$ octahedra are symbolized by the open and the solid circles corresponding to the two different configurations. This model structure belongs to the space group C2/n when the orientations of NO_2 are neglected.

Fig. 17 Comparison of the calculated structure factor of the superlattice reflections ($K_h \pm k_0$) with observed values by X-ray and neutron diffraction. R-factor is 12% (24% for superlattice reflections) with 6 parameters. The unit of the structure factor is the same as Fig. 15.

Fig. 18 The local distortion of $Cu(NO_2)_6$ octahedron of phase III shown on the Q_2-Q_3 space. The observed value is $\pm 58.6°$ measuring from the $-Q_3^z$ axis. This indicates that the local Jahn-Teller distortion is Q_3^x and Q_3^y type distortion in each sublattice.

Fig. 19 Shematic features of pseudospin state of $K_2PbCu(NO_2)_6$ shown on σ^x-σ^z space. (a) The 'fan' pseudospin state in Phase II and (b) the canted pseudospin state in Phase III.

Fig. 20 The 'phase diagram' of $R_2PbCu(NO_2)_6$ system. Lattice constants are chosen as the vertical axis and temperature are horizontal axis. Over all feature suggests that the stability of phase II are related to the distance between $Cu(NO_2)_6$ groups.

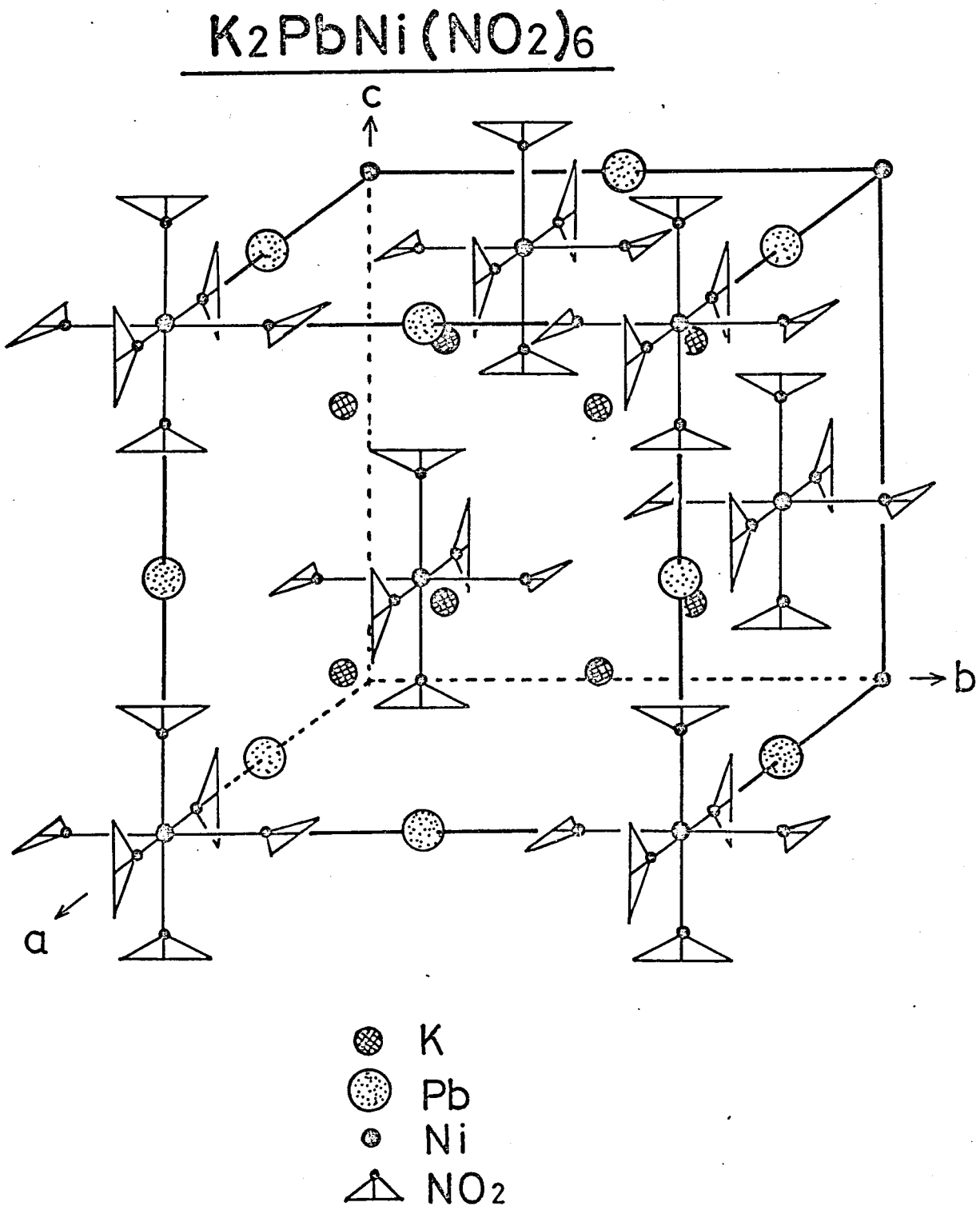

FIGURE 1

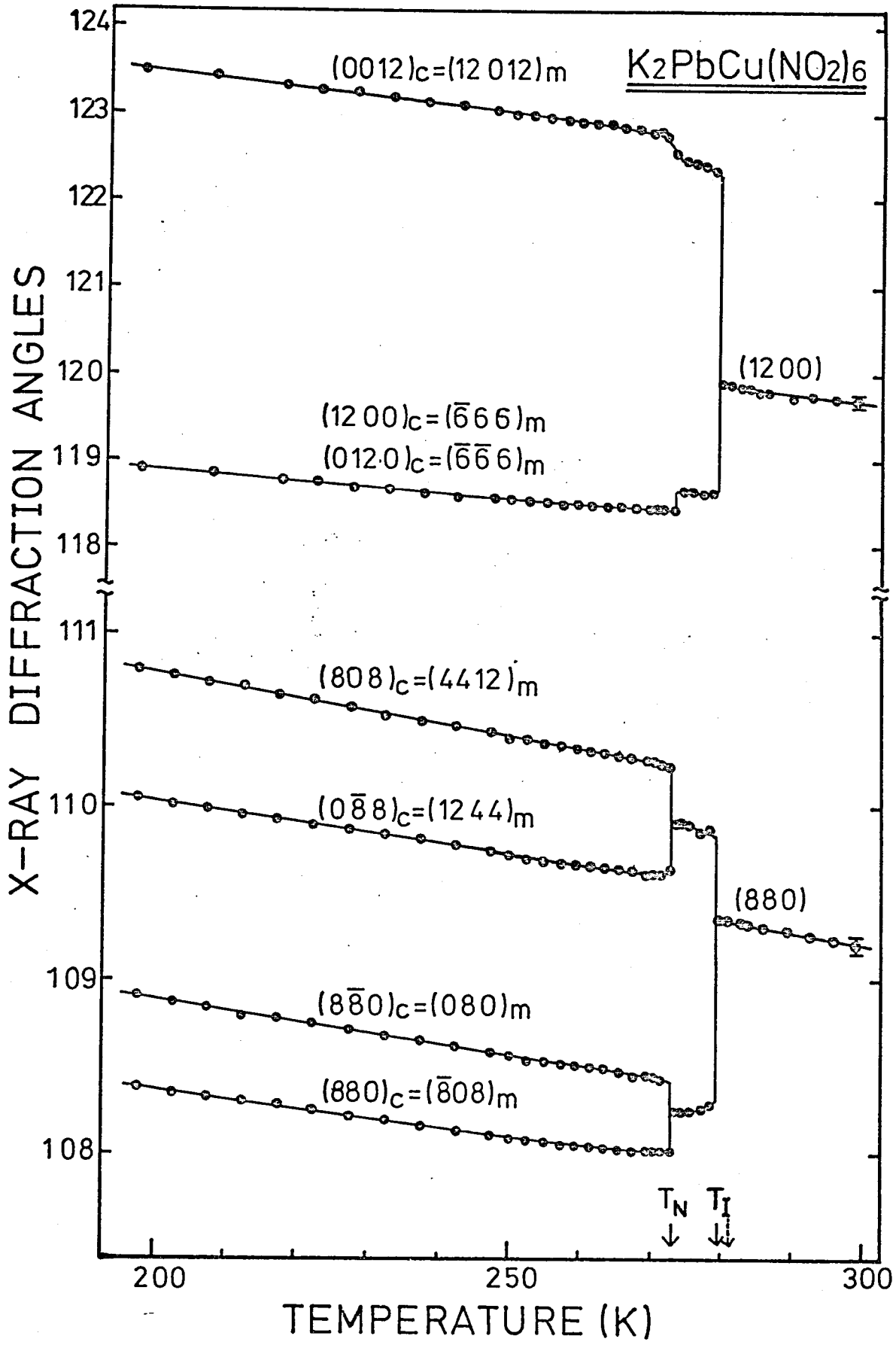
K2PbCu(NO2)6
(0012)c=(12 012)m
(12 00)
(12 00)c=(6̄ 6 6)m
(012·0)c=(6̄ 6̄ 6)m
(8 0 8)c=(4 4 12)m
(0 8̄ 8)c=(12 4 4)m
(8 8 0)
(8 8̄ 0)c=(0 8 0)m
(8 8 0)c=(8̄ 0 8)m
X-RAY DIFFRACTION ANGLES
TEMPERATURE (K)
124
123
122
121
120
119
118
111
110
109
108
200
250
300
TN
TI

FIGURE 2

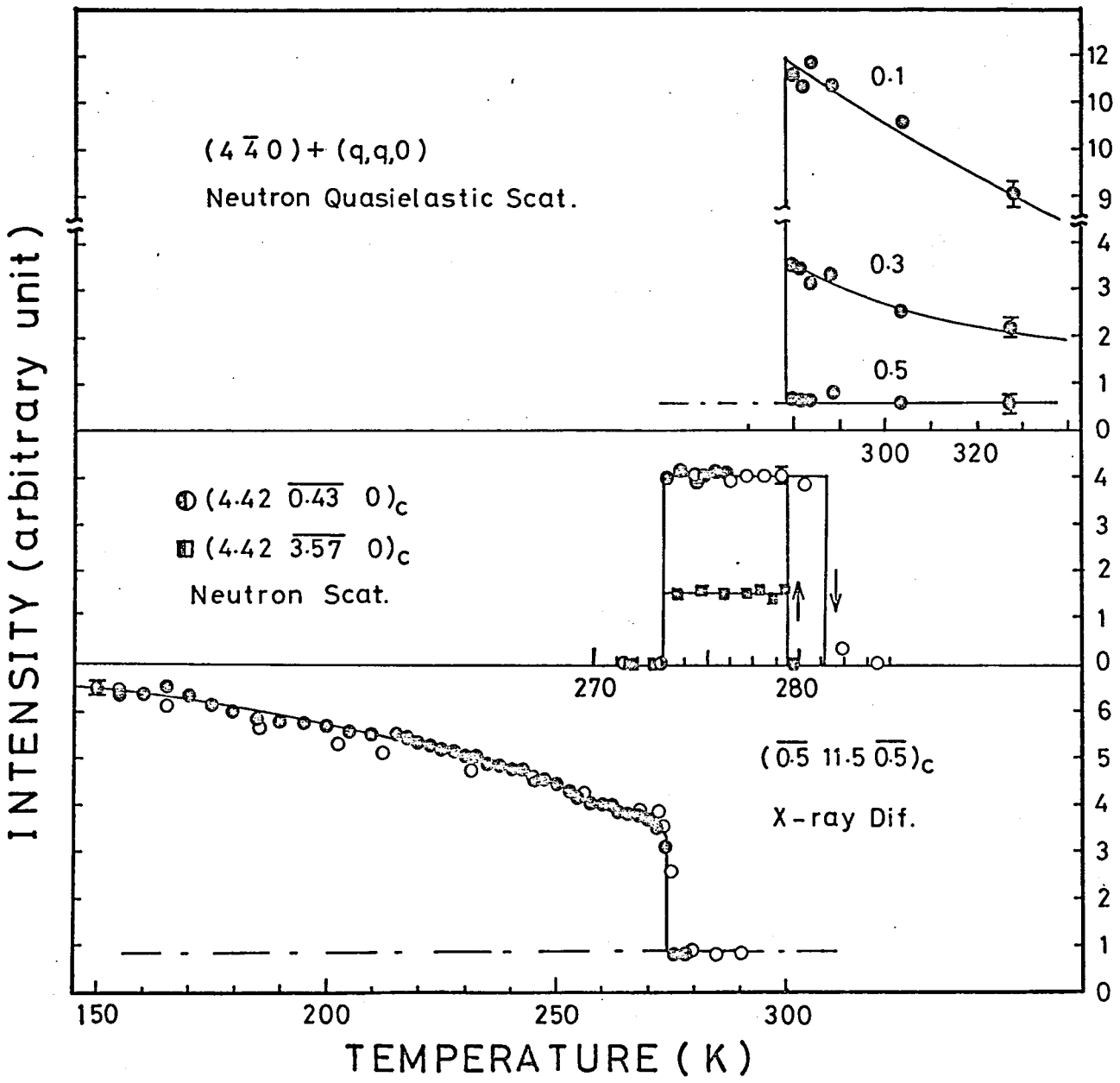
INTENSITY (arbitrary unit)
(4 $\bar{4}$ 0) + (q,q,0)
Neutron Quasielastic Scat.
0·1
0·3
0·5
300
320
① (4·42 $\overline{0·43}$ 0)$_c$
▮ (4·42 $\overline{3·57}$ 0)$_c$
Neutron Scat.
270
280
($\overline{0·5}$ 11·5 $\overline{0·5}$)$_c$
X-ray Dif.
150
200
250
300
TEMPERATURE (K)

FIGURE 3

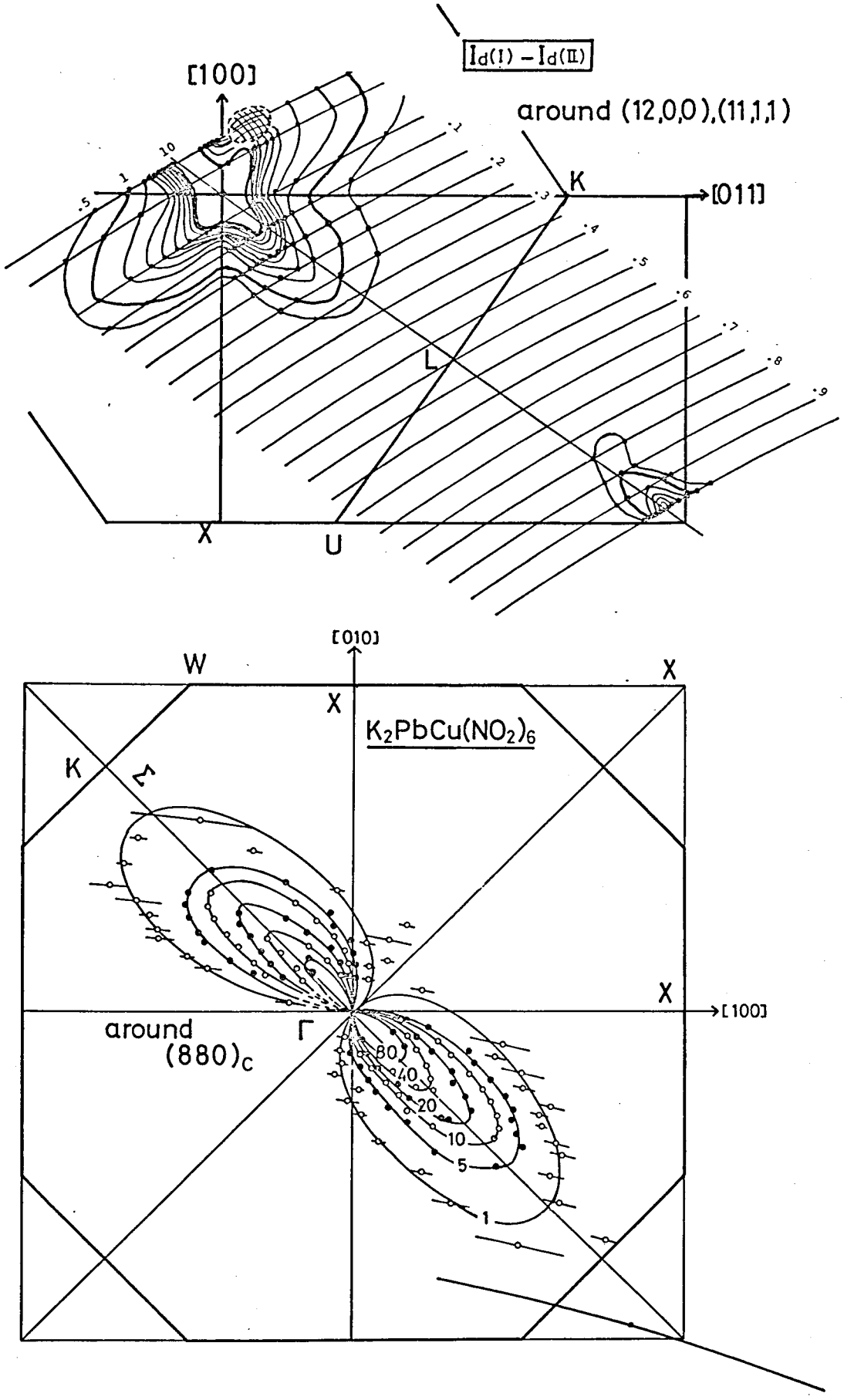
$I_{d(I)} - I_{d(II)}$
[100]
around (12,0,0),(11,1,1)
K
[011]
L
X
U
[010]
W
X
X
$K_2PbCu(NO_2)_6$
K
Σ
X
[100]
around
$(880)_C$
Γ
80
40
20
10
5
1

FIGURE 4

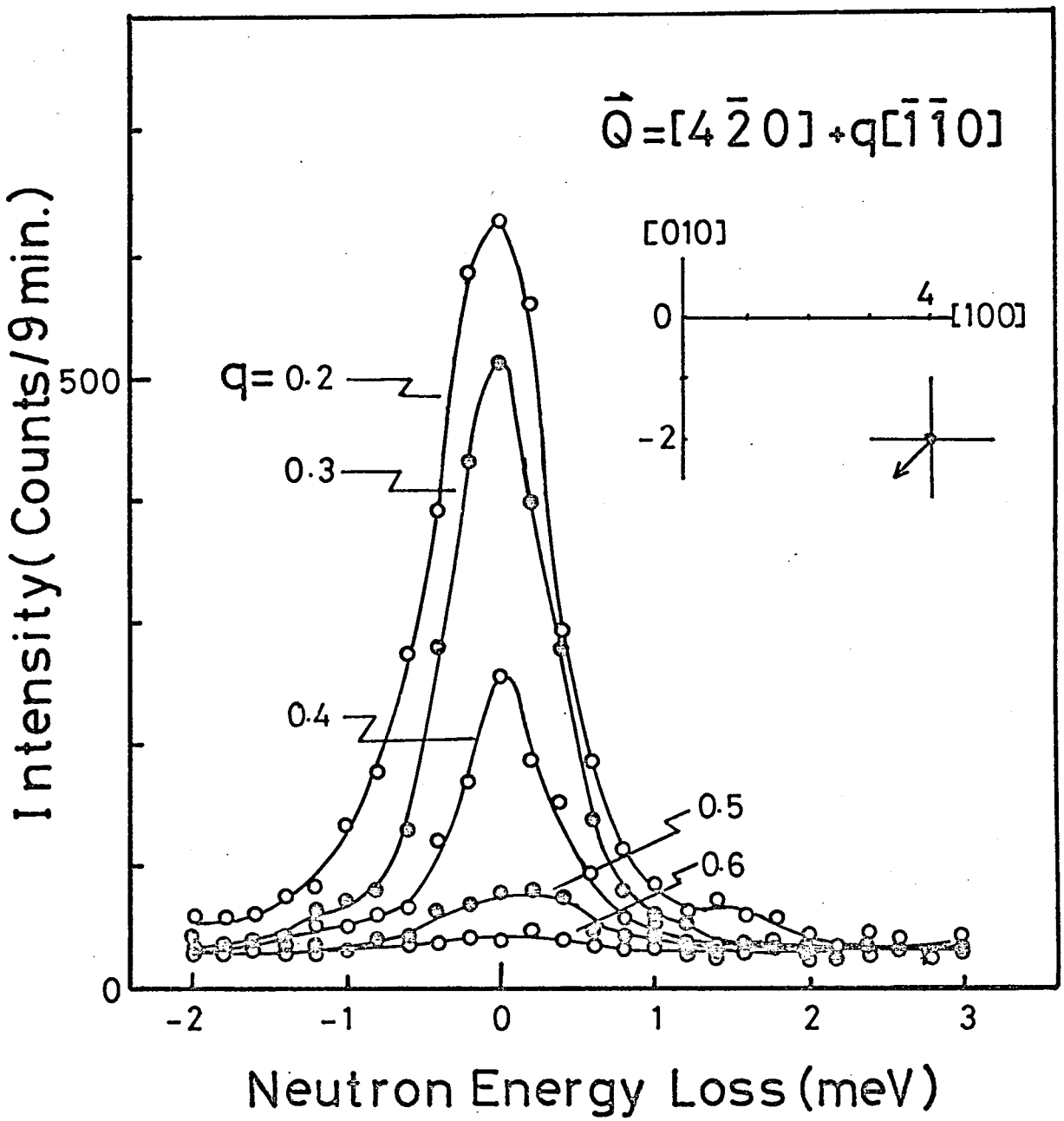
$\vec{Q}=[4\bar{2}0]+q[\bar{1}\bar{1}0]$
[010]
0
4
[100]
-2
q= 0.2
0.3
0.4
0.5
0.6
Intensity(Counts/9 min.)
500
0
-2
-1
0
1
2
3
Neutron Energy Loss (meV)

FIGURE 5

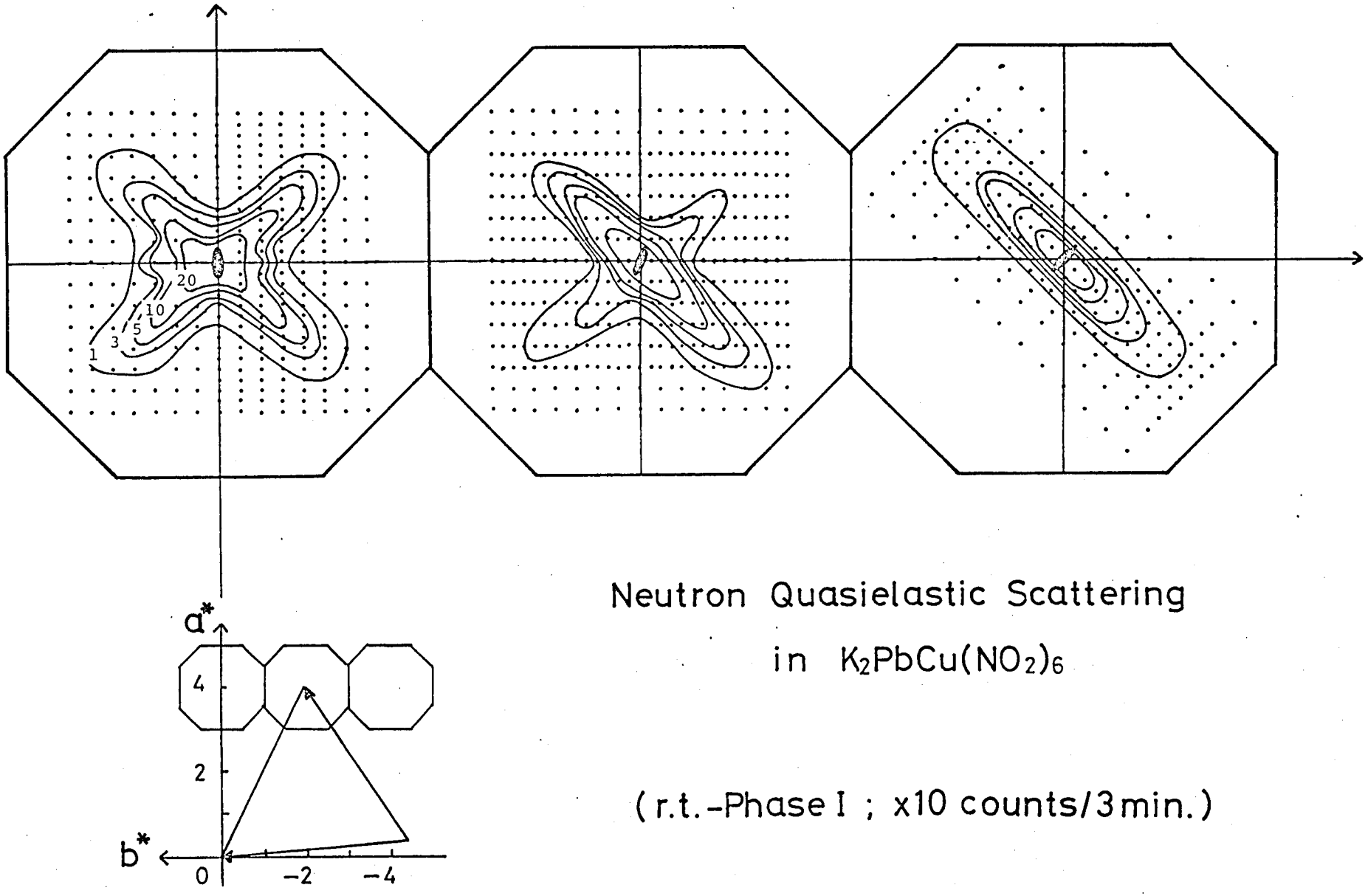

FIGURE 6

Neutron Quasielastic Scattering

in $K_2PbCu(NO_2)_6$

(r.t.-Phase I ; x10 counts/3min.)

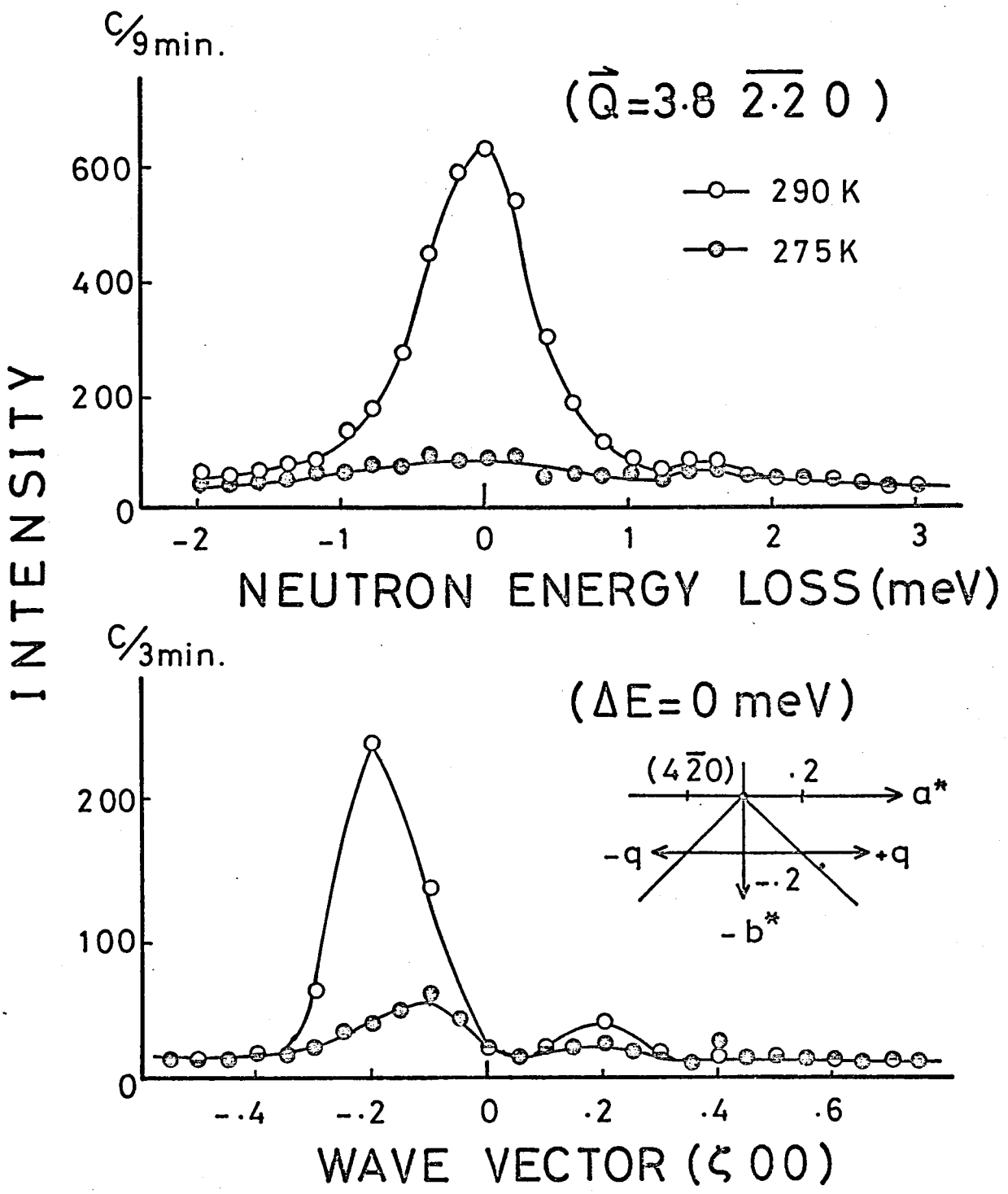
C/9min.
($\vec{Q}$=3·8 $\overline{2}$·2 0)
290 K
275K
600
400
200
0
-2
-1
0
1
2
3
INTENSITY
NEUTRON ENERGY LOSS(meV)
C/3min.
(ΔE=0 meV)
(4$\overline{2}$0)
·2
a*
-q
+q
-·2
-b*
200
100
0
-·4
-·2
0
·2
·4
·6
WAVE VECTOR (ζ 00)

FIGURE 7

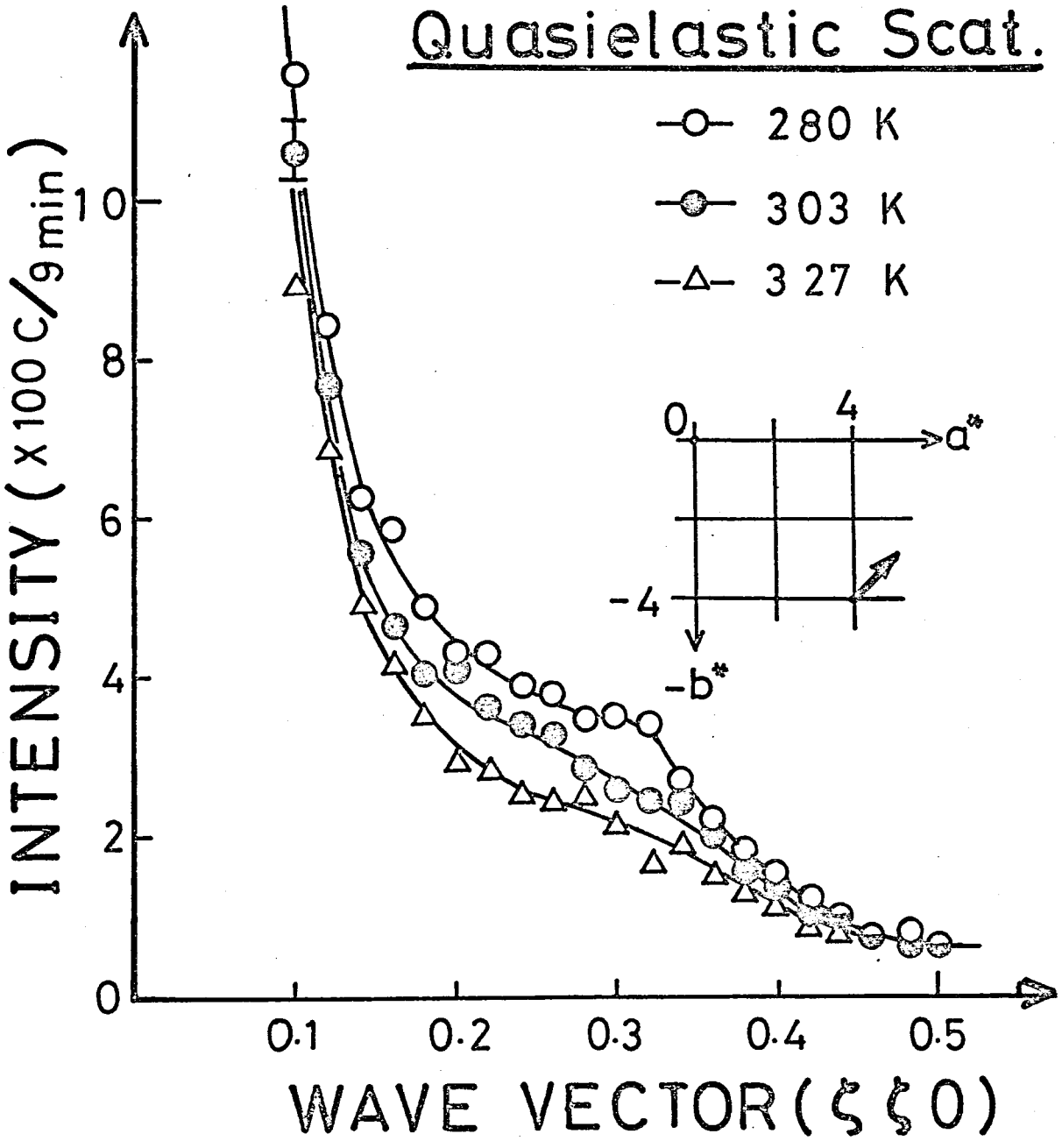
Quasielastic Scat.
280 K
303 K
327 K
INTENSITY (x100 C/9 min)
0
2
4
6
8
10
0.1
0.2
0.3
0.4
0.5
WAVE VECTOR (ζ ζ 0)
0
4
a*
-4
-b*

FIGURE 8

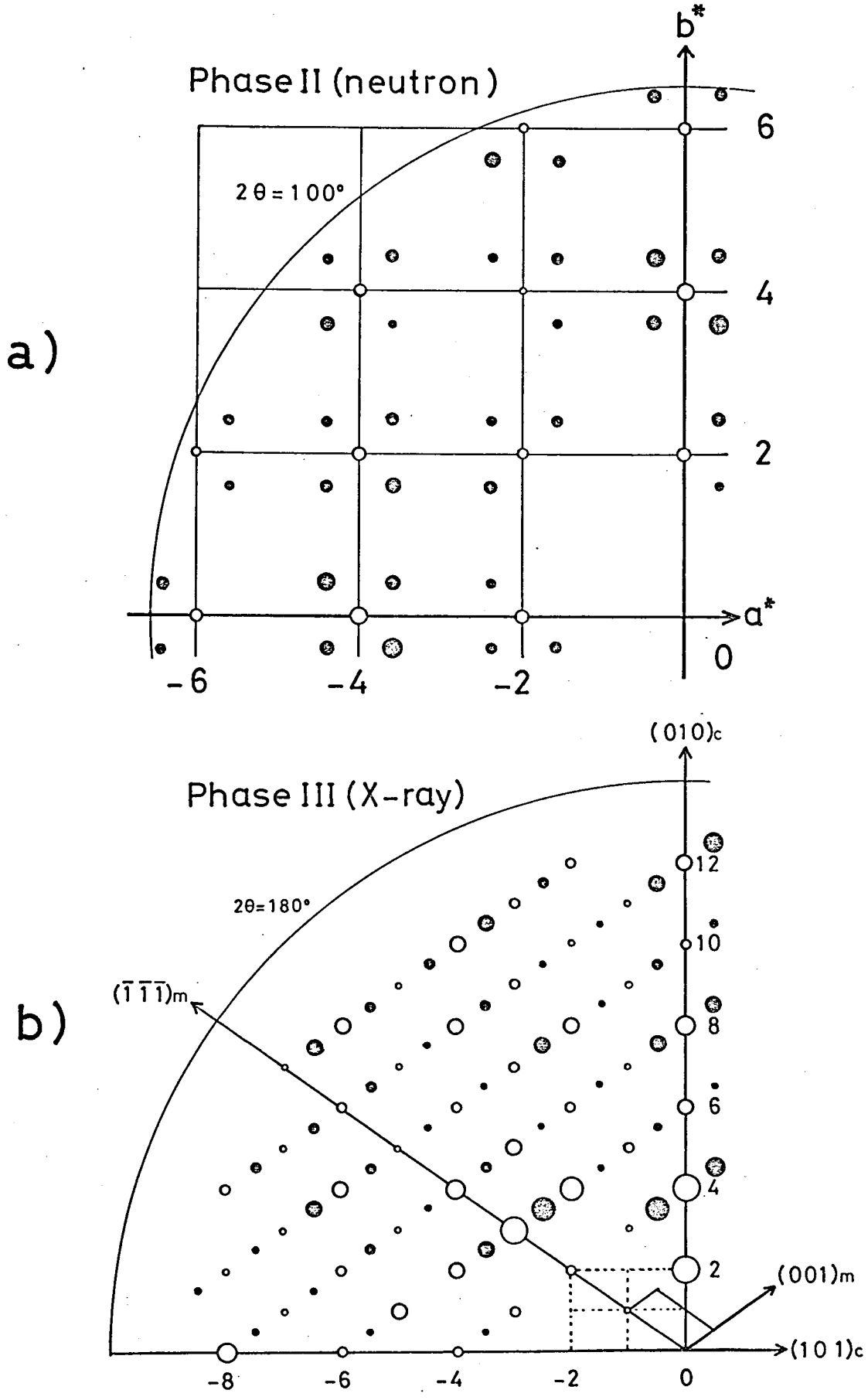
a)
Phase II (neutron)
b*
2θ = 100°
6
4
2
0
a*
-6
-4
-2
b)
Phase III (X-ray)
(010)c
2θ=180°
(1̄ 1̄ 1̄)m
12
10
8
6
4
2
(001)m
(10 1)c
-8
-6
-4
-2
0

FIGURE 9

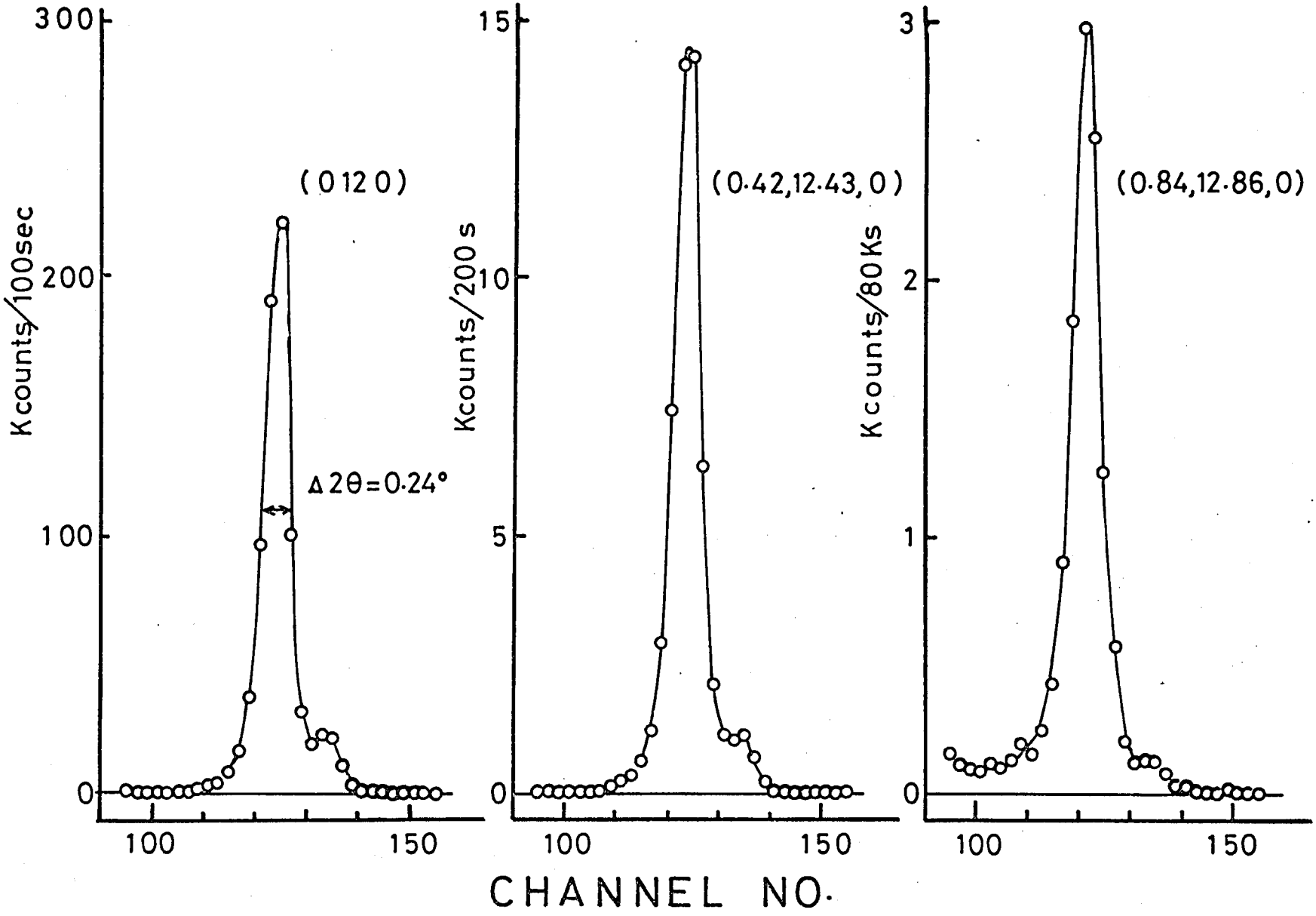
300
200
100
0
Kcounts/100sec
(0 12 0)
Δ2θ=0·24°
15
10
5
0
Kcounts/200s
(0·42,12·43,0)
3
2
1
0
Kcounts/80Ks
(0·84,12·86,0)
100
150
100
150
100
150
CHANNEL NO.

FIGURE 10

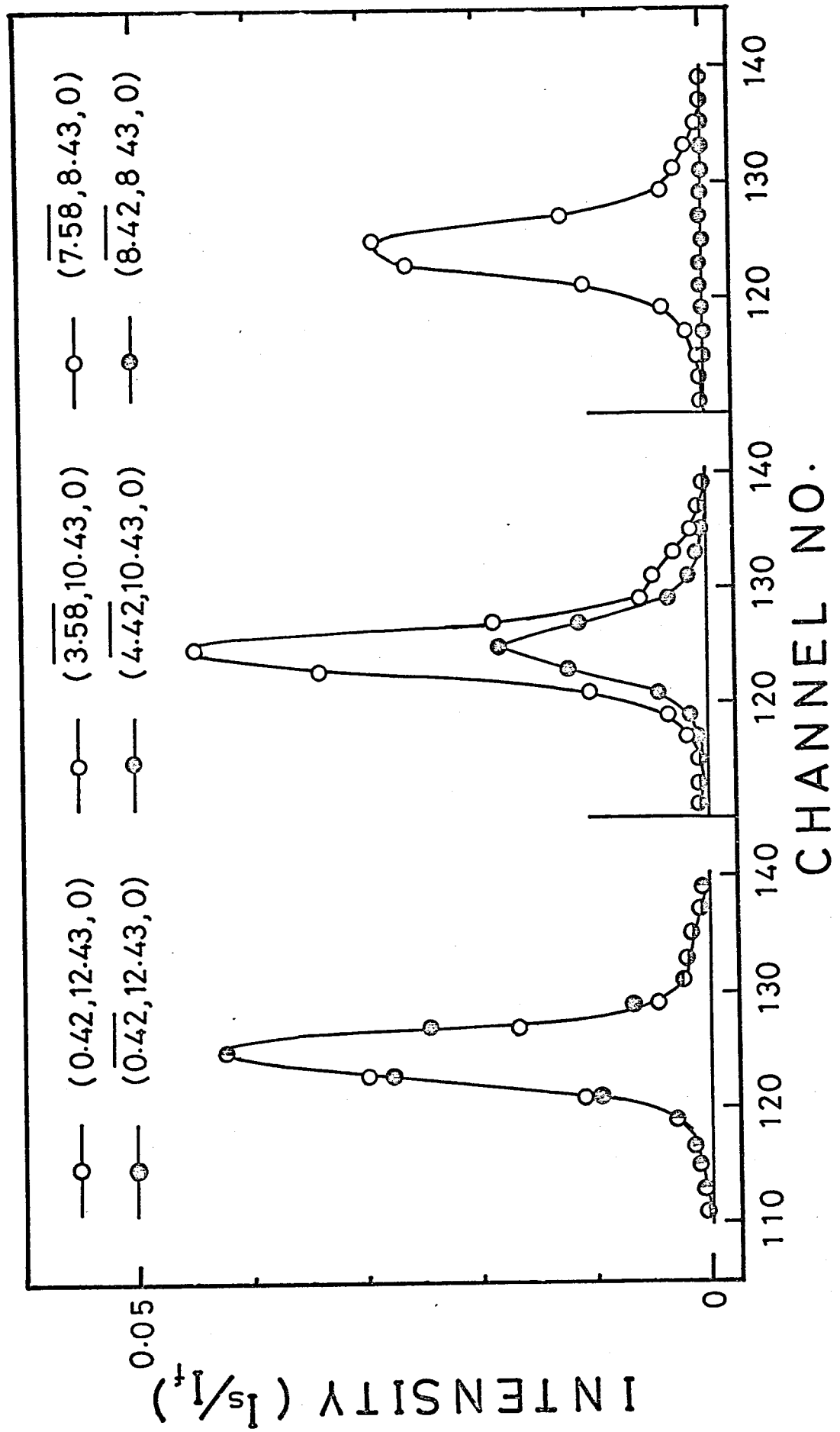
INTENSITY (I_s/I_f)
0.05
0
CHANNEL NO.
110
120
130
140
(0.42,12.43,0)
(0.$\overline{42}$,12.43,0)
($\overline{3.58}$,10.43,0)
(4.$\overline{42}$,10.43,0)
($\overline{7.58}$,8.43,0)
(8.$\overline{42}$,8 43,0)

FIGURE 11

FIGURE 12

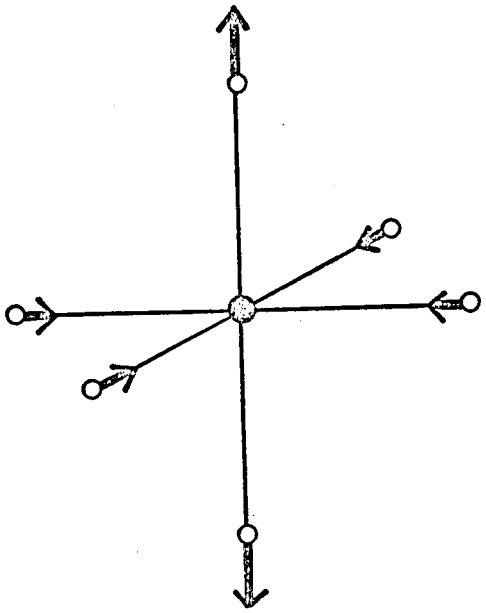

Q_3 -mode

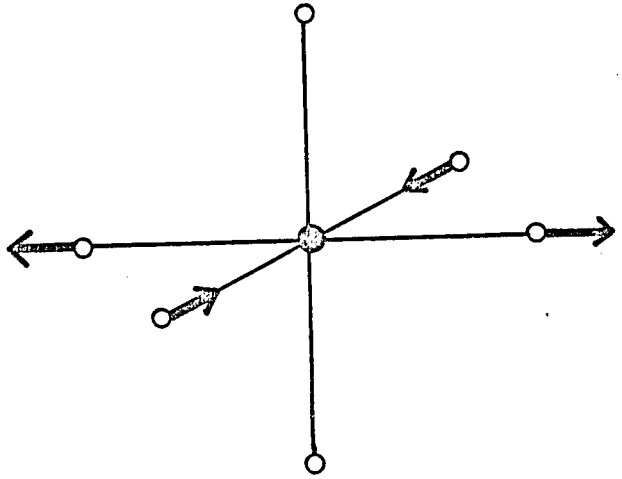

Q_2 -mode

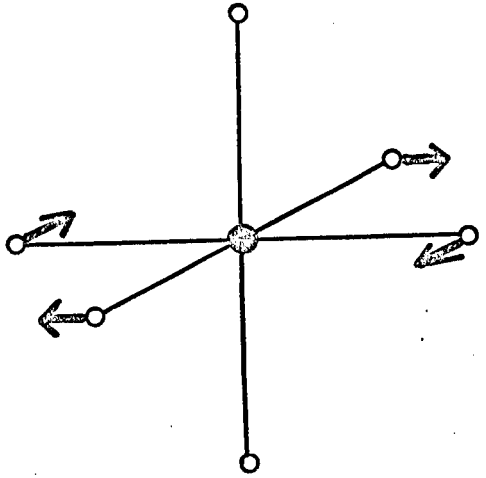

T_g -mode

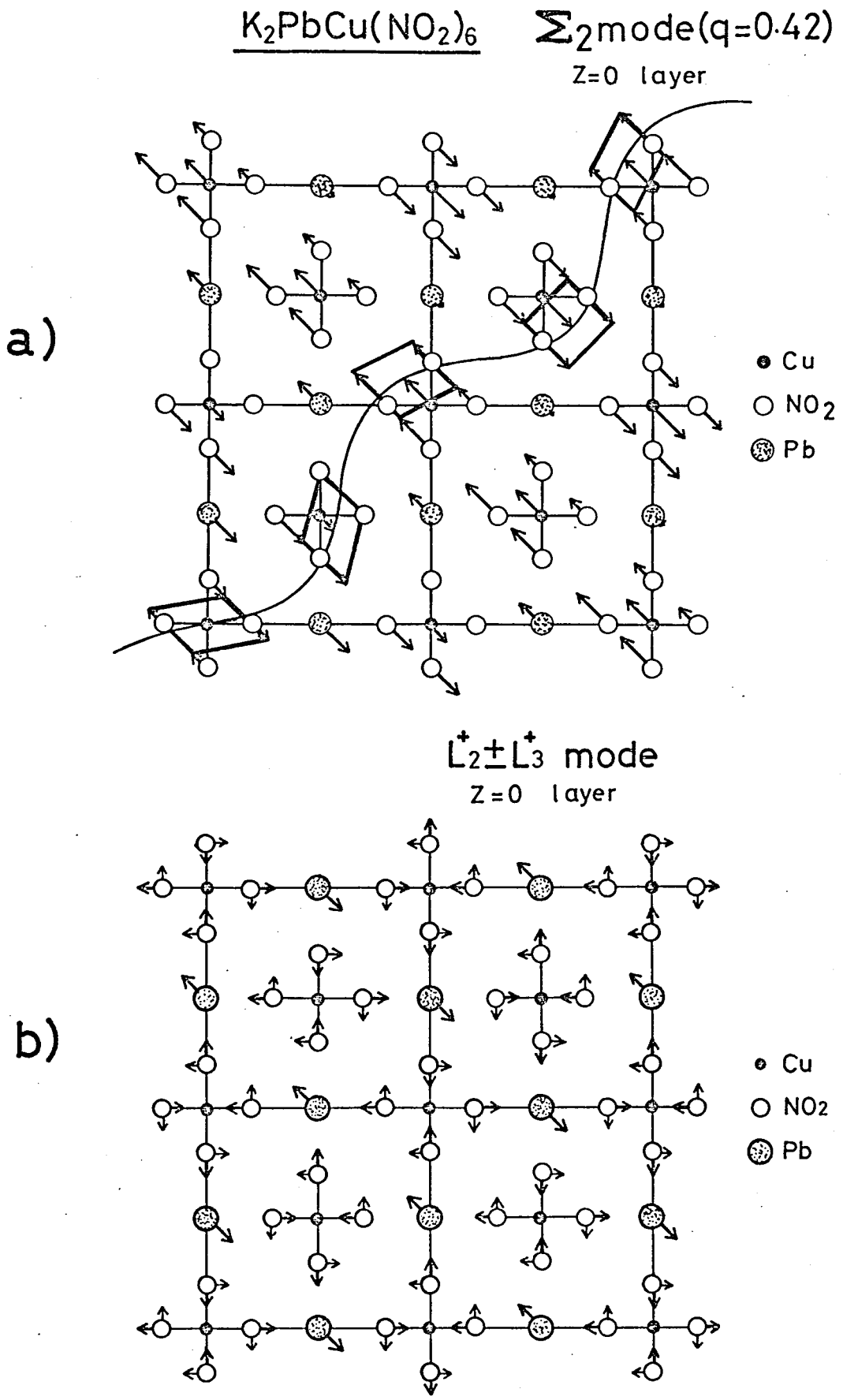
$K_2PbCu(NO_2)_6$ $\Sigma_2$mode(q=0.42)
Z=0 layer
a)
Cu
NO_2
Pb
$L_2^+ \pm L_3^+$ mode
Z=0 layer
b)
Cu
NO_2
Pb

FIGURE 13

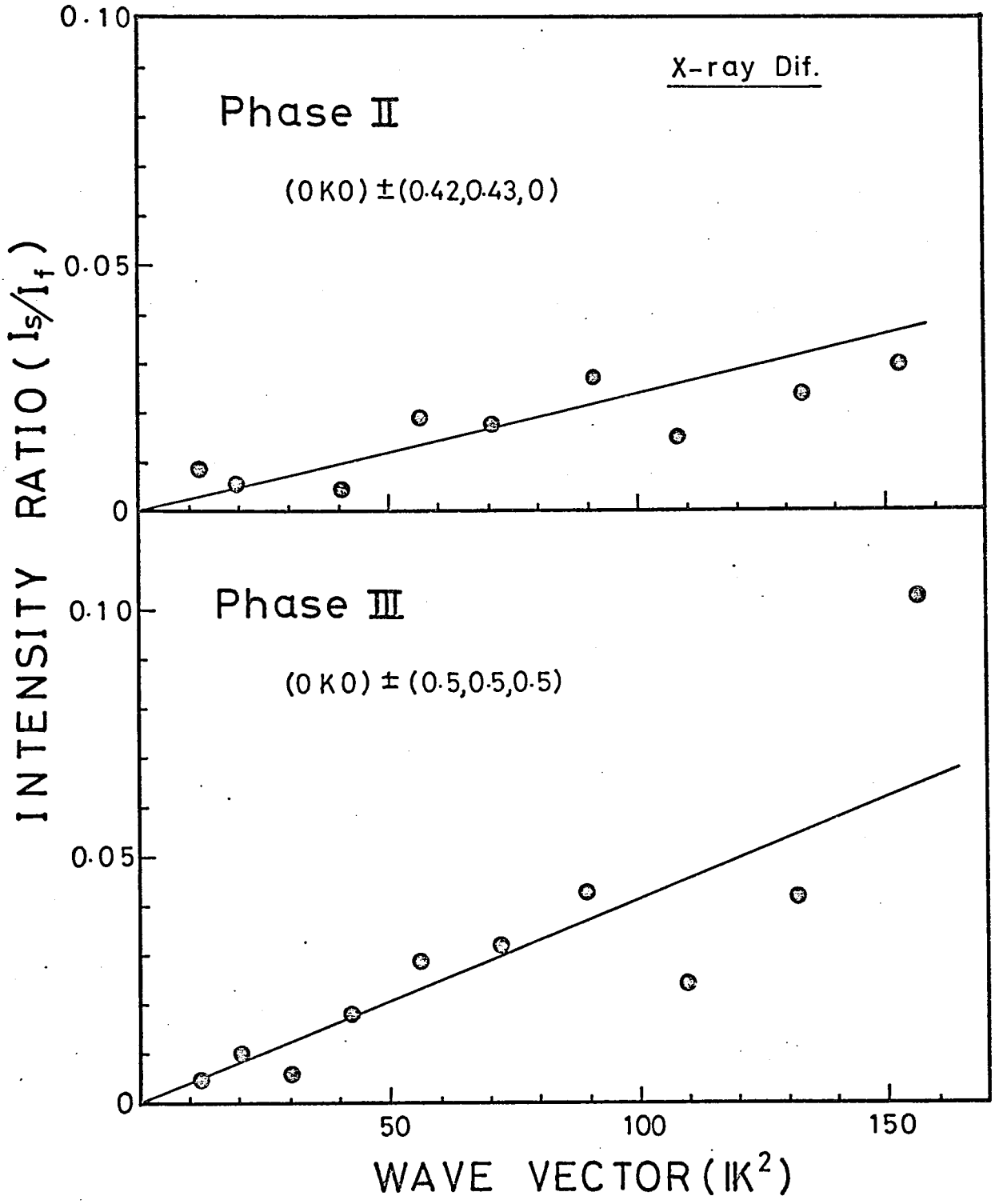
X-ray Dif.
Phase II
(0 K 0) ± (0·42, 0·43, 0)
Phase III
(0 K 0) ± (0·5, 0·5, 0·5)
INTENSITY RATIO (I_s/I_f)
0·10
0·05
0
0·10
0·05
0
50
100
150
WAVE VECTOR (IK^2)

FIGURE 14

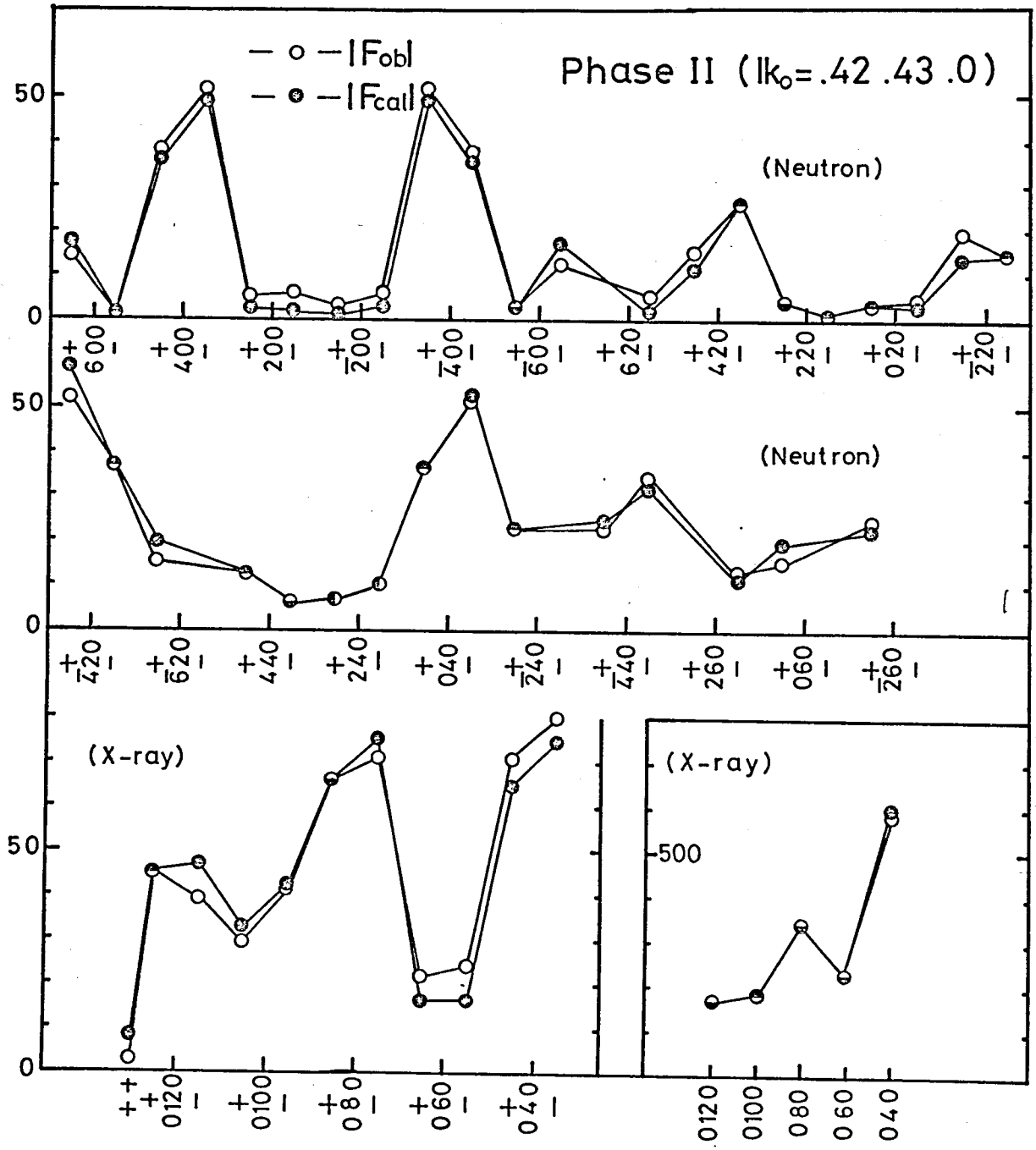
— o — |Fobl
— ⊛ — |Fcal|
Phase II (|k₀=.42 .43 .0)
(Neutron)
(Neutron)
(X-ray)
(X-ray)
500
50
0

FIGURE 15

$C\bar{1}$ (C2/n) Symmetry

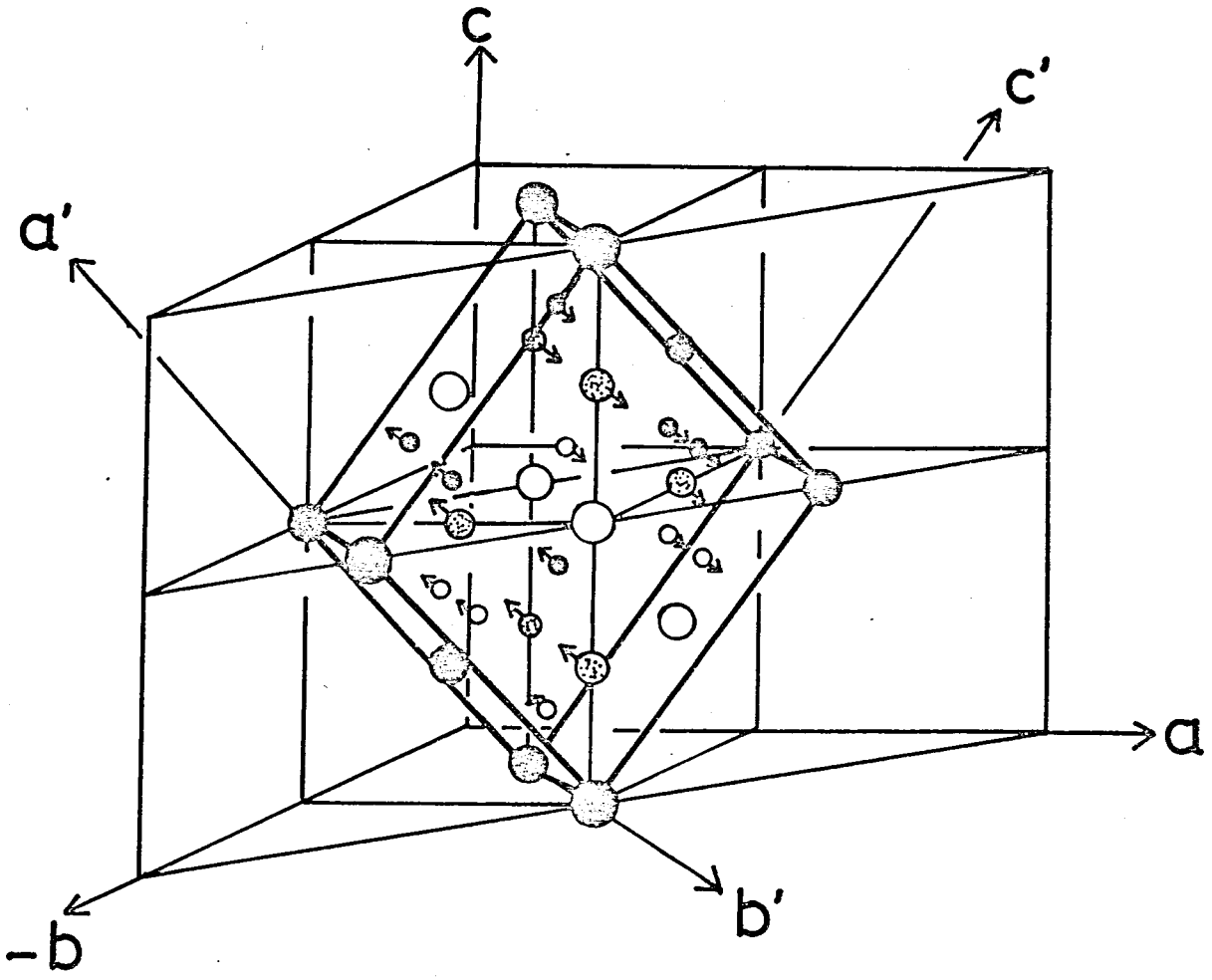

$Cu(NO_2)_6$ - A

$Cu(NO_2)_6$ - B

Pb

K_1

K_2

FIGURE 16

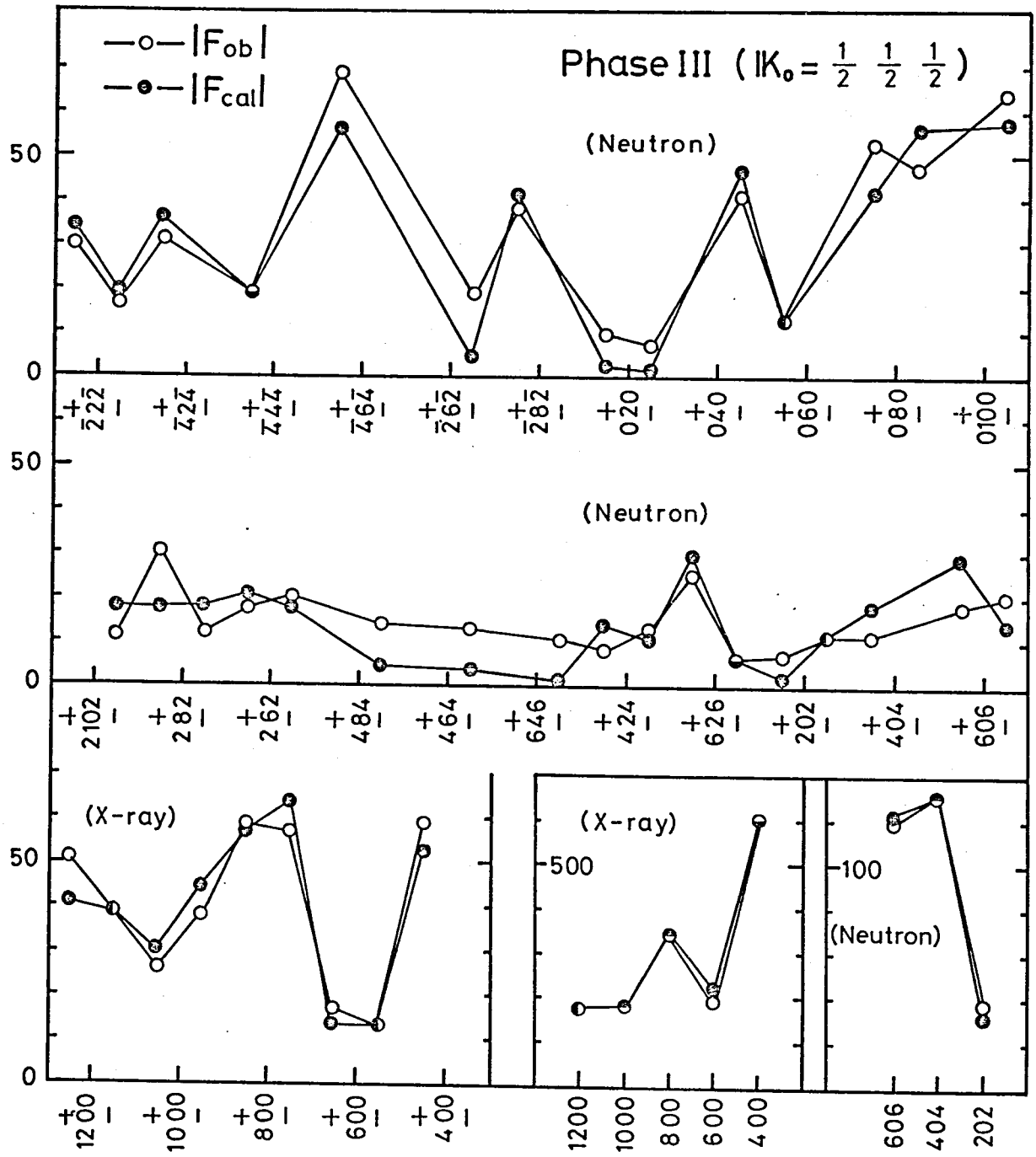
—o— |Fob|
—●— |Fcal|
Phase III ($K_0 = \frac{1}{2}\ \frac{1}{2}\ \frac{1}{2}$)
(Neutron)
50
0
$+\bar{2}\bar{2}_-$ $+\bar{4}\bar{2}_-$ $+\bar{4}\bar{4}_-$ $+\bar{6}\bar{4}_-$ $+\bar{6}\bar{2}_-$ $+\bar{8}\bar{2}_-$ $+020_-$ $+040_-$ $+060_-$ $+080_-$ $+0100_-$
(Neutron)
$+2\bar{1}0_-$ $+2\bar{8}_-$ $+2\bar{6}_-$ $+4\bar{8}_-$ $+4\bar{6}_-$ $+6\bar{4}_-$ $+4\bar{2}_-$ $+6\bar{2}_-$ $+20_-$ $+40_-$ $+60_-$
(X-ray)
500
100
(Neutron)
$+1\bar{2}00_-$ $+10\bar{0}0_-$ $+8\bar{0}0_-$ $+6\bar{0}0_-$ $+4\bar{0}0_-$
1200 1000 800 600 400
606 404 202

FIGURE 17

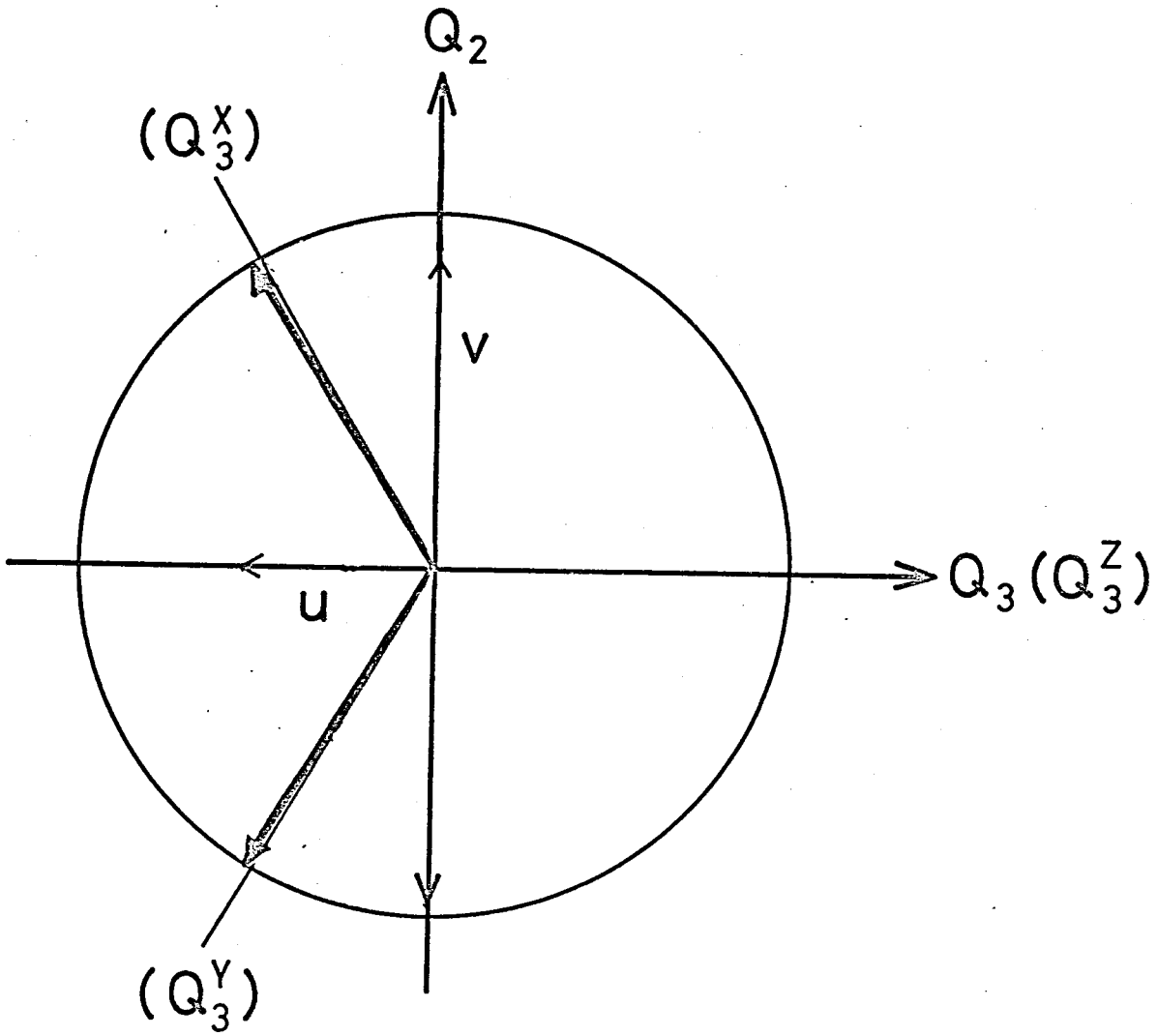

Phase III

'antiferro'
local distortion

FIGURE 18

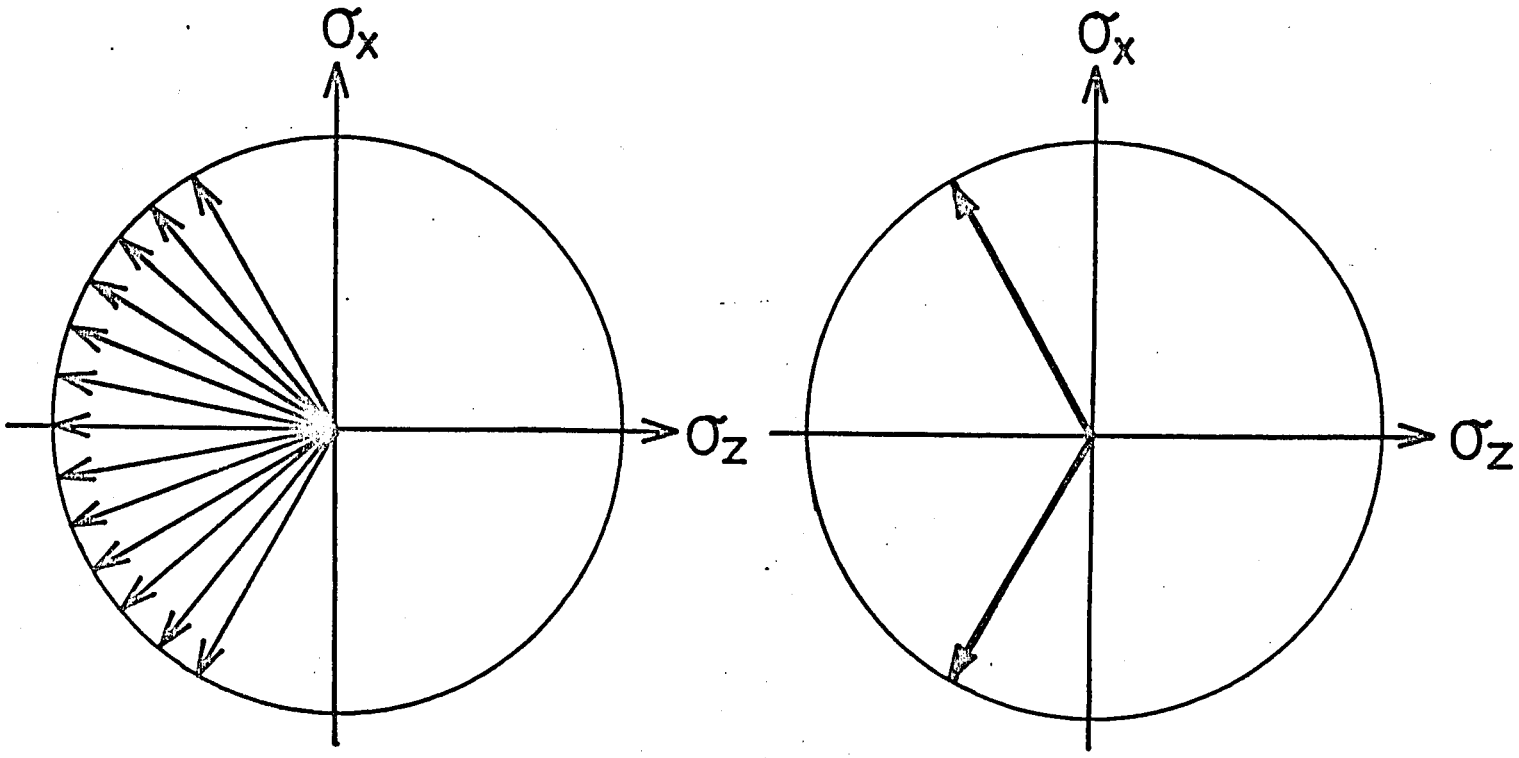

Phase II

'fan spin' structure

Phase III

'canted spin' structure

FIGURE 19

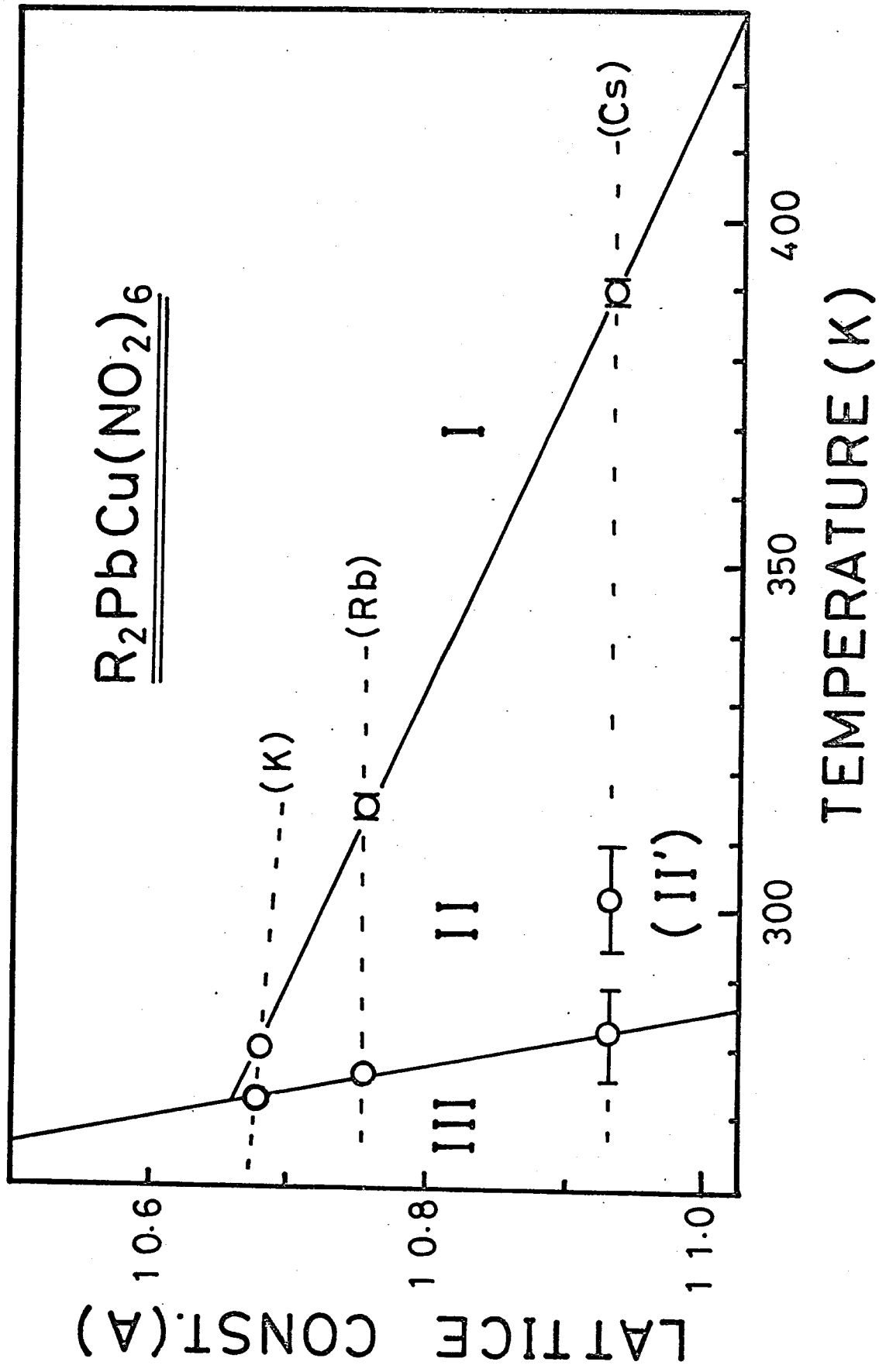
$R_2PbCu(NO_2)_6$
(K)
(Rb)
(Cs)
I
II
III
(II')
LATTICE CONST.(Å)
10.6
10.8
11.0
300
350
400
TEMPERATURE (K)

FIGURE 20